Yields and molecular composition of gas phase and secondary organic aerosol from the photooxidation of the volatile consumer product benzyl alcohol: formation of highly oxygenated and hydroxy nitroaromatic compounds

Mohammed Jaoui[1], Kenneth S. Docherty[2], Michael Lewandowski[1], Tadeusz E. Kleindienst[1]

[1]Center for Environmental Measurement & Modeling, U.S. Environmental Protection Agency, Research Triangle Park, NC, 27711, USA
[2]Jacobs Technology, Inc., Research Triangle Park, NC, 27709, USA

Correspondence: Mohammed Jaoui (Jaoui.mohammed@epa.gov)
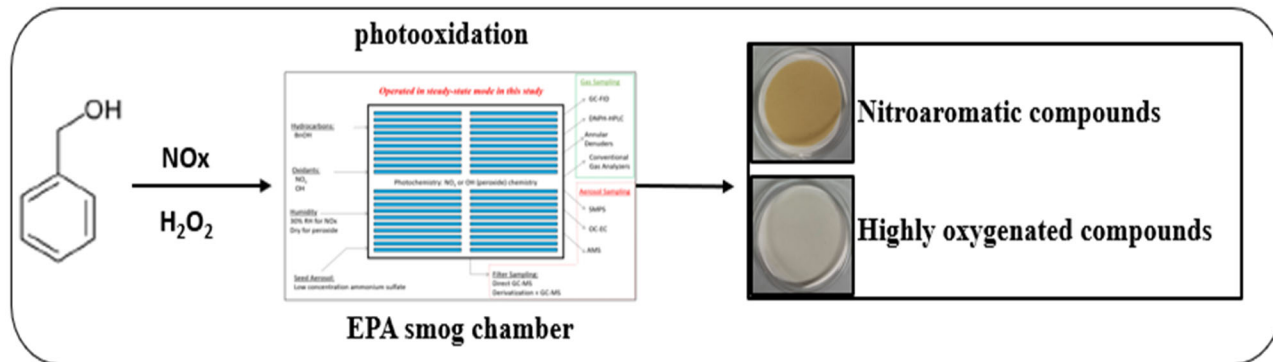
Abstract. Recently, volatile chemical products (VCPs) have been increasingly recognized as important precursors for secondary organic aerosol (SOA) and ozone in urban areas. However, their atmospheric chemistry, physical transformation, and their impact on climate, environment, and human health remain poorly understood. Here, the yields and chemical composition at the molecular level of gas and particle phase products originating from the photooxidation of one of these VCPs, benzyl alcohol (BnOH), are reported. The SOA was generated in the presence of seed aerosol from nebulized ammonium sulfate solution in a 14.5 m^3 smog chamber operated in flow mode. More than 50 organic compounds containing nitrogen and/or up to seven oxygen atoms were identified by mass spectrometry. While a detailed non-targeted analysis has been made, our primary focus has been to examine highly oxygenated and nitro-aromatic compounds. The major components include ring-opening products with high oxygen to carbon ratio (e.g., malic acid, tartaric acids, arabic acid, trihydroxy-oxo-pentanoic acids, and pentaric acid), and ring-retaining products (e.g., benzaldehyde, benzoic acid, catechol, 3-nitrobenzyl alcohol, 4-nitrocatechol, 2-hydroxy-5-nitrobenzyl alcohol, 2-nitrophloroglucinol, 3,4-dihydroxy-5-nitrobenzyl alcohol). The presence of some of these products in the gas and particle phases simultaneously provides evidence of their gas/particle partitioning. These oxygenated oxidation products made dominant contributions to the SOA particle composition in both low and high NOx systems. Yields, organic mass to organic carbon ratio, and proposed reaction schemes for selected compounds are provided. The aerosol yield was 5.2% for BnOH/H_2O_2 at SOA concentration of 52.9 µg m^{-3} and ranged between 1.7-8.1 % for BnOH/NOx at SOA concentration of 40.0-119.5 µg m^{-3}.

Key words: Benzyl alcohol, highly oxygenated compounds, Consumer products, VCPs, Silylation, Yield, Nitroaromatic compounds, SOA

1 Introduction

Modeling atmospheric organic aerosol (OA) using chemical transport models (CTMs) is complex, challenging, and often can lead to model-measurement discrepancies (Zhao et al., 2016). Applying CTMs to urban areas reveals that traditional VOCs including combustion-related processes cannot account for the observed OA mass, leaving a substantial fraction unresolved (Hayes et al., 2015). Recent studies suggest that this discrepancy is due in part to unaccounted, rapidly reacting SOA and ozone precursors from unknown sources (Hodzic et al, 2009; Hayes et al., 2015; McDonald et al., 2018; Akherati et al. 2019; Lu et al., 2020). Volatile chemical products (VCPs), such as personal care products, cleaning agents, coatings, adhesives, and pesticides have emerged as possible sources in urban areas (McDonald et al., 2018). Their emissions can be larger than those from usual sources, such as motor vehicles (Coggon et al., 2021). Laboratory, modeling, and field studies for VCPs have been conducted to assess their potential to affect ambient OA and ozone formation in urban and suburban locations (McDonald et al., 2018; Khare et al., 2018; Stockwell et al., 2021; Seltzer et al., 2021; Gkatzelis et al., 2021; Milani et al., 2021; Pennington et al., 2021; Coggon et al., 2021). The contribution of VCPs to ambient OA is not fully understood and only limited modeling studies have been reported (Mohr et al., 2015; Vlachou et al., 2018; Pennington et al., 2021; Qin et al., 2021; Seltzer et al., 2021). Additionally, few experimental and chamber studies of VCPs have been conducted with limited characterization of aerosol products (Wu and Johnston, 2016, 2017; Harrison and Well, 2012; Charan et al., 2020, 2021; Humes et al., 2022). For example, the analysis of SOA from the oxidation of cyclic methyl siloxanes (Wu and Johnston, 2016, 2017; Fu et al. 2020; Alton and Browne, 2020; Charan et al., 2021) and cyclic siloxanes (Janechek et al., 2019) has been conducted. Kinetic studies with limited products characterization have been reported for the oxidation of benzyl alcohol (BnOH) by hydroxyl radicals (Bernard et al., 2013; Wang, 2015; Harrison and Well, 2009, 2012). Recently, Humes et al. (2022) highlight the importance of oxygenated aromatic VCPs emission to generate urban SOA and oxygenated products in both gas and aerosol phases. Therefore, understanding the atmospheric chemistry of VCPs is important to assess their role in air quality and climate and to improve SOA chemistry in CTMs thereby allowing for better estimates in health studies and source apportionment.

The challenges associated with evaluating VCP impacts on urban OA can be addressed by identifying atmospheric VCP concentrations and SOA markers linking those VCP to ambient particulate matter (PM). Benzyl alcohol (C_7H_8O) is an important ring containing VCP used as an organic intermediate and a solvent in a wide range of applications (Antonelli et al. 2002). BnOH is emitted also from flowers and flowering trees (Do et al., 1969; Horvat et al., 1990; Larsen and Poll, 1990; Humpf and Scheier, 1991; Boatright et al., 2004; Vallat and Dorn, 2005; Orlova et al.; 2006) and found in indoor

77 air (Weschler, 2011). Gas kinetic studies of loss rates and product distributions have been conducted using flow tubes and

78 environmental chambers. Bernard et al. (2013) examined the rate and mechanisms of the OH + BnOH reaction. Similarly,

79 Harrison and Wells (2009, 2012) investigated the rate constants for the BnOH reaction with ozone, OH and NO_3 radicals.

80 Carter et al. (2005) conducted chamber experiments to assess ozone and PM formation from BnOH and related

81 compounds. Product studies from BnOH oxidation have focused mainly on gas phase (GP) products. Several carbonyl

82 products (benzaldehyde (BnAld), formaldehyde, glyoxal, butenedial, 4-oxopentanal, 3-hydroxy-2-propanaldehyde), and

83 benzyl nitrate, o-hydroxybenzyl alcohol, o-dihydroxy benzene were reported from the above studies. With respect to the

84 particle phase (PP), Charan et al. (2020) reported aerosol yields from BnOH oxidation together with a limited number of

85 SOA products. Finally, Wang (2015) conducted a theoretical study to elucidate the reaction mechanism of the oxidation

86 of BnOH with OH radicals.

87   In this study, we report a detailed non-targeted chemical analysis of GP and SOA products originated from the

88 photooxidation of BnOH in the presence and absence of oxides of nitrogen (NOx), with the aim to better understand the

89 chemical composition at the molecular level. Gas chromatography-mass spectrometry (GC-MS) and high-performance

90 liquid chromatography were used for the identification of a range of organic compounds including oxygenated

91 nitroaromatics and related compounds bearing up to seven oxygen atoms. Nitroaromatics are pollutants of concern due to

92 their toxicity, light-absorption properties, and relatively long residence times in the environment. Highly oxygenated

93 compounds can partition into pre-existing particles or be involved in new particle formation. Also, in the present study,

94 SOA and secondary organic carbon (SOC) yields were measured with the results compared to published data. A chemical

95 mechanism is then proposed to represent and account for selected gas- and aerosol-phase products observed in this study.

96

97 **2 Experimental methods**

98   All chemicals including N, O-*bis*(trimethylsilyl) trifluoroacetamide (BSTFA) derivatization reagent with 1%

99 trimethylchlorosilane (TMCS) as catalyst and benzyl alcohol (99%), 2-methyl-4-nitrophenol, L-(+)-tartaric acid, D-(-)-

100 tartaric acid, and meso-tartaric acid were purchased from Aldrich Chemical Co. (Milwaukee, WI) at the highest purity

101 (99.8%) available and were used without further purification. In addition to standards reported in our previous studies

102 (Jaoui et al., 2004; 2018), 3-nitrobenzyl alcohol, benzoic acid, and 4-nitrocatechol were purchased from Tokyo Chemical

103 Industry (OR, USA); while pentaric acid, 2,3-dihydroxy-4-methoxy-4-oxobutanoic acid, and arabic acid were obtained

104 from Aurum Pharmatech, LLC (NJ, USA).

2.1 Chamber description and operation

All experiments were conducted in a 14.5 m^3 fixed-volume chamber having TFE Teflon coated walls and maintained at a positive pressure of 0.1 Torr. The chamber operation, procedures, and instrumentation have been described previously (Kleindienst et al. 2006; 2009), and here just experiment-specific details are primarily included. A combination of fluorescent bulbs having radiation from 300-400 nm was used to photolyze NO_2. In the absence of NO_x, the radiation system was altered to include UV-313 sunlamps to adequately photolyze H_2O_2. The chamber was operated in steady-state (SS or flow) mode to provide continuously stable effluent concentrations. Under these conditions, reactants and products equilibrate with the chamber surfaces to minimize irreversible losses of gases and particles. The SS operation allows for extended sampling periods to improve the accuracy and precision of the measurements (Shilling et al., 2008). Temperature, relative humidity, and UV light intensity were measured continuously with an uncertainty of 5%. Pre-experiment and post-experiment procedures (see section 2.5 below) were routinely carried out before and after each experiment to minimize contamination in the chamber. The reactant generation system provided constant sources of zero air, reactants, water vapor, and ammonium sulfate (AS) seed aerosol. The reactant flow of gases (e.g., NO_x) into the chamber was regulated using mass flow controllers. BnOH was injected using a syringe pump, vaporized in a heated glass bulb, and injected with zero air. For experiments in the absence of NOx, a 50% aqueous solution of H_2O_2 was vaporized and injected using a second syringe pump, and photolyzed to produce OH radicals. Typical chamber AS concentrations were approximately 1 μg m^{-3}. Each SS experiment went through an initial transient period of 18-24 h until the reactant and product concentrations reached steady state.

2.2 Gas-phase measurements

A wide variety of instruments were used to measure the reactants and products. Nitric oxide (NO) and NOx were measured with a TECO (Franklin, MA) oxides of nitrogen analyzer with an upstream nylon filter to remove nitric acid produced from OH + NO_2. The NOx analyzer was calibrated with a NIST-traceable NO standard. Initial H_2O_2 concentrations were estimated by UV absorption using the ratio of the H_2O_2 to O_3 absorbances at 254 nm, as described by Kleindienst et al. (2009). Experiments in the absence of NOx were conducted dry to avoid aqueous loss of H_2O_2. BnOH concentrations in the inlet and within the chamber were measured semi-continuously using an SRI Model 8610C compact gas chromatograph with flame ionization detector (GC-FID; SRI Instruments, Torrance CA). The purity of the BnOH was verified with GC-MS analysis.

133   Low molecular weight carbonyls and dicarbonyls were quantified by derivatization using 2,4-dinitrophenylhydrazine

134   (Smith et al., 1989). Samples were collected at 0.5 L min^{-1} for 25 min and derivatized in a 4 mL solution of acidified

135   DNPH and then heated for 40 min at 70°C. Air samples were drawn for 20 min at a rate of 0.50 L min−1 through an

136   impinger containing 5 mL of a DNPH solution in acetonitrile. The resulting solutions were analyzed by high-performance

137   liquid chromatography with a ultraviolet detector (HPLC/UV) (Smith et al., 1989). A 15-component hydrazone standard

138   (comprising formaldehyde-, acetaldehyde-, acrolein, acetone-, propionaldehyde-, crotonaldehyde-, methacrolein-,

139   butyraldehyde-, 2-butanone-, BnAld-, glyoxal-, valeraldehyde-, m-tolualdehyde-, methylglyoxal-, and hexaldehyde;

140   AccuStandard, Inc.) at a free carbonyl concentration of 30 μg mL^{-1} for each component was used for calibration. Separate

141   dihydrazone standards of glyoxal-DNPH and methylglyoxal-DNPH were also formulated. Carbonyls were separated

142   using a Hewlett-Packard (HP) 1100 HPLC system having an Agilent Zorbax ODS 4.6 x 250 mm, 5-μm column maintained

143   at 30°C eluted with binary acetonitrile-water gradient. A 10 μL injection volume was used for all standards and samples.

144   Carbonyls were quantified by UV absorption with a diode array detector set to 360 nm. Control and sample processing

145   were managed with HP ChemStation software. More highly oxidized gas-phase organic species were also collected with

146   a 60-cm, 4-channel XAD4-coated annular denuder for off-line analysis (Jaoui and Kamens, 2001). Once collected, the

147   denuders were extracted and analyzed according to the methodology described in section 2.4 below.

148

149   **2.3 Aerosol-phase: bulk parameter measurements**

150   Organic carbon (OC) was measured using a semi-continuous elemental carbon-organic carbon (EC-OC) instrument

151   (Sunset Laboratories, Tigard, OR) (Offenberg et al., 2007). The pumping system draws chamber effluent through a quartz

152   filter at a rate of 8 L min^{-1} with carbon-strip denuder to remove gas-phase organics that might interfere with the

153   measurement. With a sample collection time of 0.5 h and an analysis time of 0.25 h, the duty cycle for the measurement

154   of OC was 0.75 h (Lewandowski et al., 2015). The aerosol volume, size distribution, and total number density were

155   measured using a scanning mobility particle sizer (SMPS), (Model 3071A, TSI, Inc., Shoreview, MN) and a condensation

156   particle counter (CPC) (Model 3010, TSI, Inc., Shoreview, MN). The SMPS operating conditions were as follows: sample

157   flow 0.2 L min^{-1}; sheath flow 2 L min^{-1}; size scan from 19 to 982 nm.

158

159   **2.4 Molecular characterization of GP and PP oxygenated organic products**

160   A non-targeted chemical analysis was conducted focusing mainly on species bearing hydroxy and carboxylic groups

161 (Jaoui et al., 2004, 2013, 2018). For each experiment, six 47-mm glass fiber (GF) filters were taken for 24 h at a flow rate

162 of 16.7 L min^{-1}. A second set of samples used an in-line 60-cm XAD-4 coated annular denuder (followed by a GF filter)

163 and analyzed for gas-phase organic products (Jaoui and Kamens, 2001). After collection, GF filters were extracted by

164 sonication with 5 mL methanol for 1 h, and denuders were extracted with 30 mL 1:1 dichloromethane/methanol mixture

165 (Jaoui and Kamens, 2001). Prior to extraction, denuders and GF filters were spiked with *cis*-ketopinic acid (KPA), trans-

166 p-menth-6-ene-2,8-diol (PMD), and d$_{50}$-tetracosane (TCS) as internal/recovery standards (IS/RS). Denuder extraction

167 solvents were rotary evaporated to ~1 mL and filtered using 0.45-μm PTFE syringe filters. A 2 μL portion of this extract

168 was analyzed by GC-MS (Jaoui and Kamens, 2001). The remaining denuder and filter extracts were evaporated to dryness

169 under a gentle stream of N$_2$ at room temperature using an N-Evap evaporation bath (Organomation Associates, Inc.,

170 Berlin, MA), then derivatized with BSTFA (Jaoui et al., 2004). This technique provides a sensitive method for measuring

171 low levels of highly oxidized organic compounds, including semi- and intermediate-volatile compounds in the GP and

172 PP.

173   The GC-MS analysis was conducted on an Agilent GC (7890B) coupled with a quadrupole mass spectrometer

174 (5977B). The injector, heated to 270 ^{o}C, was operated in splitless mode. Compounds were separated on a 60-m-long, 0.25-

175 mm-i.d. RTx-5MS column (Restek, Inc., Bellefonte, PA) with a 0.25-μm film thickness. The GC oven temperature was

176 initiated at 84 ^{o}C, held for 1 min, then increased at 8 ^{o}C min^{-1} to 200 ^{o}C, followed by a 2-min hold, then an increase at 10

177 ^{o}C min^{-1} to 300 ^{o}C and a 15-min hold. The ion source, ion trap, and interface temperatures were 200, 200, and 300 ^{o}C,

178 respectively. Mass spectra were collected in both the methane-chemical (CI) and electron ionization (EI) modes.

179

180 **2.5 Experimental and quality control procedures**

181   Before each experiment started, the chamber was flushed with zero air (hydrocarbon-free) for 24 h from an Aadco

182 clean generator (Cleves, OH, USA). Experiments were conducted in either the absence or presence of NOx. For

183 experiments with NOx, BnOH and NO were added to the chamber through flow controllers to the target concentration.

184 For experiments in the absence of NOx, the photolysis of H$_2$O$_2$ was the source of OH. H$_2$O$_2$ as a 50 % aqueous solution

185 was injected through a syringe pump into a heated glass bulb where it vaporized and then was mixed rapidly by the main

186 dilution air flow. For these experiments, BnOH was added as described above. Ammonium sulfate seed aerosol was also

187 introduced into the chamber for all experiments to serve as a condensing medium for semivolatile organic products that

188 might form. After the reactants reached steady state concentrations (24 hours), the background was characterized using

189 all instruments to check for artifacts including background GP and PP species. Background chamber air was also

190 characterized using off-line analysis of denuder and/or filters as described above. Previous studies show that BnAld and

191 to a lesser extent benzoic acid, benzyl benzoate and dibenzyl ether present either as impurity, or as decomposition products

192 upon BnOH exposure to air at room temperature or sonication (Urakami et al., 2000; Ferri et al., 2006; Abend et al., 2004).

193 Here we investigated the effect of chamber air, sonication, and BSTFA derivatization on BnOH artifacts as described in

194 the supplementary information (SI) in section 1. A small amount of BnAld impurity was detected using the direct injection

195 (DI) method and estimated to be <0.1% in the purchased solution. When BnOH was exposed to clean air in the chamber

196 in the absence of light, sonication, and/or BSTFA derivatization, our results show additional low level of BnOH

197 conversion to BnAld and benzoic acid using DI and BSTFA methods, which is similar to the findings of Abend et al.

198 (2004), Urakami et al. (2000), and Ferri et al. (2006). Additional results and descriptions are provided in section S1 (SI).

199 Experiments were initiated by turning on the lights and allowing the irradiated chamber effluent to reach SS

200 conditions over a 24-h period which permits active sampling by the on-line instruments and the collection of denuder and

201 filter samples for subsequent off-line analysis. For organic intermediates wall losses are typically not an issue due to

202 reactions being conducted within a Teflon chamber. This potential issue is mitigated further from operating the chamber

203 in a SS mode where compound loss and re-evaporation quickly comes to steady state. Short lifetimes of radical

204 intermediates with other gas-phase constituents also render a negligible wall-loss. The stability of BnOH in the chamber

205 was investigated and BnOH was found to be highly stable with results given in the SI (section S1). Denuders and GF filter

206 samples were also analyzed to probe reproducibility of the analytical technique. The analysis showed consistent results.

207 Gas and particle samples from BnOH photooxidation are dominated by oxygenated species, several not having

208 authentic standards, and thus a portion of each sample was derivatized. Initially, we eliminated peaks detected in blank

209 and background samples. For compounds having standards, comparisons were made between the retention times and mass

210 spectra (CI and/or EI mode) of the chamber-derived peaks and those of the standards. For compounds not having

211 standards, individual peak identifications were associated with a product peak only if its retention time and mass spectrum

212 was consistent with the fragmentation pattern of the BSTFA-derivatized compound. All recorded spectra in this study

213 were compared with those derived from reference standards, the literature, the NIST library, and an archive of mass

214 spectra from product compounds determined in our laboratory over the past twenty years.

215

3 Results and discussion

The initial conditions of the experiments conducted in this study are summarized in Table 1. Three NOx experiments were carried-out with initial BnOH ranging from 0.36 – 0.72 ppm and NO from 0.096 – 0.19 ppm. One experiment without NO_X was conducted with initial H_2O_2 and BnOH levels of 3.0 and 0.32 ppm, respectively. NOx experiments were conducted at ~30% RH, and the H_2O_2 experiment at < 4% RH to minimize H_2O_2 uptake onto chamber surfaces. Chamber temperatures were set to 25 °C. Each experiment was conducted for up to five days for samples requiring substantial masses or extended collection times and frequencies.

Steady state concentrations of NO, BnOH, O_3, and NOy for the four experiments are given in Table 2. The reacted BnOH and NO were calculated from the difference between the initial and steady-state concentrations. For NOx experiments, the range of reacted BnOH concentrations was 0.22 – 0.34 ppm having a reproducibility of 20–30%. Under these conditions, steady state concentrations of NOy, and O_3 were in the range of 0.08 – 0.16 and 0.011 – 0.15 ppm, respectively. With NO present at steady-state, peroxy-peroxy (RO_2–RO_2) reactions were minimized. A constant aerosol source was maintained for initial conditions given in Table 1. The major aerosol parameters measured (SOA, SOC, and OM/OC) are given in Table 3. SOC uncertainties were taken from the reproducibility of the semi-continuous measurement and typically better than 10% for a single run. For the organic mass (OM), the uncertainties are determined from the reproducibility of side-by-side filter measurements which are typically better than 5%. An estimate of the systematic errors due to minor changes in reactant concentrations, minor variations in chamber temperature, and similar factors bring the total uncertainty to between 15-25% for these parameters (Kleindienst et al., 2009). SOA/SOC values were then determined from the corrected data and given in Table 3. For experiments in the presence of NOx, SOA/SOC values ranged from 1.7-2.0. Similarly, in the absence of NOx, the measured SOA/SOC value was 2.1.

3.1 Secondary organic aerosol and secondary organic carbon yields

Secondary organic aerosol yield (Y_{SOA}) and secondary organic carbon yield (Y_{SOC}) were calculated from the following respective relationships $Y_{SOA} = SOA/\Delta HC$ (1); $Y_{SOC} = SOC/\Delta HC_C$ (2) where SOA is the corrected organic aerosol mass concentration originated from filter measurements (6 filters) and ΔHC is the reacted BnOH concentration. SOC is the organic carbon concentration found in Table 3 and HC_C is the reacted BnOH carbon concentration. SOA and SOC were corrected for wall loss to the chamber which had previously been determined for organic aerosol to be 0.067 h^{-1} (Kleindienst et al. 2012). The wall loss rate is based on mass and not on the size distribution of the particles.

244   Uncertainties in the yield come from the experimental uncertainties in SOA and SOC production and the reacted BnOH

245   concentrations. The uncertainty in the reacted BnOH results from the reproducibility of the initial and steady-state values

246   and is estimated to range from 20 - 30% given the low volatility of BnOH and challenges for introducing oxygenated

247   species into the chamber in a consistent manner. Such challenges are also present in a batch mode experiment given the

248   difficulty to determine BnOH time profiles given its volatility and high reactivity toward oxidants (Shilling et al., 2008;

249   Kroll et al., 2007). Similar findings have been reported for sesquiterpenes oxidation (Jaoui et al., 2013). As a result,

250   aerosol yields of higher accuracy are often reported to be associated with steady state as opposed to batch mode

251   experiments (Shilling et al., 2008). Moreover, in this work we explored the possibility of BnOH being taken up by

252   ammonium sulfate (AS) seed aerosol prior to start of the irradiation or by SOA after it is initiated. This test was conducted

253   using GC-MS analysis of derivatized (BSTFA) and underivatized denuder and GF filter extracts collected before and after

254   the reaction starts (SI; Section S1). Under the experimental conditions used in this study, BnOH was undetected in AS

255   and SOA, thus limiting any participation in particle chemistry that may occur.

256   The production of aerosol, and thus the yield, were found to be highly sensitive to the precise initial conditions (Tables 1,

257   3). Yields for the four experiments are shown in Table 3. Y_{SOA} values were determined for SOA concentrations from 39.6

258   - 119.5 µg m^{-3} and ranged between 3.6 and 8.1%. Similarly, Y_{SOC} was measured for SOC concentrations from 23.2 – 58.9

259   µgC m^{-3} and found to range between 2.7 and 5.1%. In the absence of NO_X, SOA and SOC yields were 5.2 and 3.1 %

260   measured for SOA and SOC concentrations of 52.9 µg m^{-3} and 24.8 µgC m^{-3}, respectively. For the two systems at similar

261   SOA concentrations ER890 and ER892, the SOA yield was higher for the experiment with NO_X. This may result from

262   the reaction of BnOH with NOx which tends to produce high levels of BnAld (Table 4), which may undergo secondary

263   reactions leading to additional SOA formation (see section 3.3). The BnOH reaction with NO will occur when the reaction

264   of RO_2 with NO is competitive to ring closure. Regardless, according to Wang (2015) the reaction of NO_2 with R1

265   (Scheme 1) will occur only to a minor degree compared with ring closure. As expected, the data in Table 3 indicate that

266   Y_{SOA} and Y_{SOC} are lower at the lower SOA and SOC concentrations, respectively.

267   These SOA and SOC yields can be compared with other studies. Recently, Charan et al. (2020) reported SOA yields

268   for the photooxidation of BnOH in the presence of NO_X with the initial OH coming from the photolysis of H_2O_2. Their

269   chamber was operated in a batch mode and SOA yields approaching unity were reported. By contrast, three additional

270   studies reported much lower SOA yields of 9%, 30%, and 41% from McDonald et al. (2018), Carter et al. (2005), and Li

271   et al. (2018), respectively. The yield reported by McDonald et al. (2018) was based on a multi-generation oxidation model;

that of Carter et al. (2005) was estimated as described in the original report, and that of Li et al. (2018) was based on measurements in the presence of NOx and a surrogate urban hydrocarbon. The results of our study are much closer in value to McDonald et al. (2018). The study by Charan et al. (2020) suggests that conditions can be found where BnOH SOA yields are substantially greater than that found in this study and those previously reported. The major differences between the Charan et al. study and the present work were the chamber-mode operation, the seed aerosol type and levels, and the mix of oxidants used. While it can be difficult to compare the yields from the two studies some comments can be made. (1) As noted, the Charan et al. yields result from conventional batch mode irradiations of BnOH, H_2O_2 and NOx. (2) SOA levels were measured using an SMPS which measures aerosol volume which is then converted to aerosol mass using a density of 1.4 µg nL^{-1}. (3) Perhaps the biggest difference between the two studies is the use of an extremely high initial seed aerosol mass, approximately two orders of magnitude higher than in this study. Thus, it is possible that an adsorption mechanism played a part in contributing to the measured yields. (4) Finally, the use of high initial H_2O_2 concentrations relative to BnOH make it possible that H_2O_2 effectively competed with BnOH for OH via the reaction of $OH + H_2O_2 \rightarrow HO_2 + H_2O$ thus generating a system rich in HO_2. Thus, aging process may be more prominent than in our study. The uncertainties associated with SOA and reacted BnOH measurements and wall loss correction are unlikely to account for the differences in the two studies. However, SOA yields have been reported to increase considerably as a function of initial seed aerosol (Zhang et al. 2014), as well as to increase with the OH radical exposure (Wang et al., 2018). Qualitatively these two factors might bring the present SOA yields into reasonable agreement with Charan et al. (2020), when data were extrapolated to similar seed aerosol and OH exposures. And as previously noted, in the low initial seed aerosol used in our study no benzyl alcohol was detected in the seed aerosol or deposited on SOA. As further plausibility for the results from the present study, Humes et al. (2022) recently reported yields from 12% - 18% for two oxygenated aromatic species (1-phenoxy-2-propanol, and phenoxy-ethanol), compounds having similar structures to BnOH.

3.2 Reaction products identification

Three methods were used in this study to identify oxygenated reaction products at the molecular level: (1) DNPH as derivatizing agent for small carbonyls (Smith et al. 1989); (2) BSTFA as derivatizing agent for hydroxyl and carboxylic compounds for GP and PP (Jaoui et al., 2004); and (3) direct injection (DI) method providing the capability for analysing slightly polar to non-polar compounds without the use of derivatization (Jaoui and Kamens, 2001). For the BSTFA and

300   DI methods, the analysis of laboratory generated GP and PP products from BnOH oxidation shows a series of organic

301   compounds containing nitro, ketone, carboxylic acid, and/or alcoholic functional groups. Many of these compounds do

302   not have authentic standards and their identifications were based on the interpretation of the mass spectra of the derivatized

303   and/or underivatized compound (Jaoui and Kamens 2001; Jaoui et al., 2004, 2005). The identification should be regarded

304   as tentative except for compounds that have authentic standards. For the BSTFA method, the recognition of characteristic

305   ions was used to guide the analysis of mass spectra of the derivatives obtained in both electron ionization (EI) and chemical

306   ionization (CI) using methane as reagent gas. BSTFA reacts with -COOH and -OH groups to form BSTFA derivatives.

307   Characteristic ions are m/z 73, 75, 147, and 149. Adduct ions in CI from the derivatives include m/z $M^{+\cdot} + 73$, $M^{+\cdot} + 41$,

308    $M^{+\cdot} + 29$, and $M^{+\cdot} + 1$; fragment ions include m/z $M^{+\cdot} - 15$, $M^{+\cdot} - 73$, $M^{+\cdot} - 89$, $M^{+\cdot} - 117$, $M^{+\cdot} - 105$, $M^{+\cdot} - 133$, and/or

309    $M^{+\cdot} - 207$. The approach used for the identification is as follows: peaks detected in blank and background chamber samples

310   were eliminated first. A peak was associated with a reaction product only if its corresponding mass spectrum was

311   consistent with the fragmentation pattern of the BSTFA derivatization reagent. All recorded spectra were compared with

312   spectra derived from various reference compounds, authentic standard, NIST library, the PubChem website

313   (pubchem.ncbi.nlm.nih.gov), and/or by MS assignment. While the off-line technique is an integrated technique that

314   requires long sampling times, it does provide a sensitive method for products identification at the molecular level as well

315   as measuring low concentrations of highly oxidized organic compounds, and semivolatile compounds in the GP. Thus,

316   products found by this collection technique could be informative for possible precursors for the types of compounds that

317   may form in the PP. In the following discussion, data are first presented to support tentative identifications of oxidation

318   products in the GP and PP.

319   **Gas phase products.** GP measurements were made of major carbonyl products formed during the photooxidation of

320   BnOH including formaldehyde, acetaldehyde, acetone, methacrolein, 2-butanone, BnAld, glyoxal, and methylglyoxal.

321   Steady-state concentrations are given in Table 4. Under the conditions shown in Tables 1 and 2, high concentrations were

322   observed for BnAld and glyoxal, and to a lesser extent formaldehyde in experiments with NOx, and high concentrations

323   of formaldehyde, acetaldehyde, and to a lesser extent BnAld and glyoxal in the experiment without NOx. BnAld level

324   was a factor of ~5 higher in NOx experiments compared to H_2O_2 experiments, and formaldehyde a factor of ~36 lower.

325   Glyoxal and methylglyoxal concentrations largely were similar in both NOx and H_2O_2 experiments. The formation of

326 BnAld, glyoxal, and formaldehyde as major products (Table 4) have already been reported from the oxidation of BnOH

327 with yields of 25 (± 5), 20 (± 2), and 3.0% (± 0.2), respectively (Bernard et al., 2013; Harrison and Wells, 2012).

328   GP samples were also collected on five-channel annular deuders. Each denuder sample was extracted and analyzed

329 directly with GC-MS without derivatization. The remaining extract was silylated, and GC-MS analyzed qualitatively.

330 Typical total ion chromatograms (TIC) of GP products detected and identified in this study are shown in Figure 1. Figure

331 1 shows portions of three TIC in +EI of GP samples taken from experiments ER889 at steady state (underivatized: Figure

332 1a), ER892 (underivatized: Figure 1b), and ER889 (silylated derivatives: Figure 1c). Peaks assigned in Figure 1 were

333 identified either by comparison with an authentic standard or by MS assignment. For clarity, only the main products are

334 shown, although several peaks could not be structurally identified. SOA generated from BnOH photooxidation is

335 dominated by oxygenated ring-opening products (see below). However, ring-retaining products were among the main

336 products observed in the GP including semivolatile organic compounds (SVOCs) (Figure 1c). Chromatograms associated

337 with the underivatized samples (Figure 1a, b) were used mainly to identify BnOH and BnAld in the system, although

338 several additional peaks absent in the background chromatogram were observed. At steady state, BnOH was not reacted

339 completely as it was detected in both systems only in the GP using both DI and BSTFA methods (Figure 1). BnAld was

340 detected in both systems in the gas and particle phases, although it was not present with BSTFA method because of the

341 absence of OH or COOH groups. Figure S3 shows EI mass spectra of BnAld identified using authentic standard, and

342 those associated with three peaks eluting at 11.3, 12.0, and 12.8 min. Although no structural information could be

343 associated with these three peaks, molecular weights of 152, 152, 138 Da (all derivatized and underivatized masses are

344 Dalton (Da) but are not designated as such hereafter), were tentatively obtained.

345   Select GP products containing OH groups identified in the present study are summarized in Table 5. Table 5 contains

346 proposed structures, molecular weights of the silylated derivatives (MW_{BSTFA}) and underivatized compounds (MW),

347 formula, and the 5 most intense ions associated with BSTFA derivatives in EI mode. Table 5 shows if GP products are

348 detected also in the PP. Figure S4 shows EI mass spectra associated with selected peaks observed in Figure 1c, including

349 BnOH-1TMS, benzoic acid-1TMS, catechol-2TMS, and 2-hydroxybenzyl alcohol-2TMS. 2-Hydroxybenzyl alcohol-

350 2TMS (2OHBnOH) peak eluted at 21.4 min was one of the largest peaks detected in the chromatogram in Figure 3c. The

351 2OHBnOH-2TMS EI mass spectrum (Figure S4, bottom) shows strong characteristic fragments ions at m/z 73, 179 ($M^{+\cdot}$

352 - 89), 253 ($M^{+\cdot}$ - 15), 268 ($M^{+\cdot}$), and its corresponding CI mass spectrum shows ions at m/z 253 ($M^{+\cdot}$ - 15), 179 ($M^{+\cdot}$ - 89)

353   and weak adducts at $M^{+\cdot} + 1$, $M^{+\cdot} + 29$, and $M^{+\cdot} + 41$ that are consistent with the presence of two (-OH) groups, indicating

354   a BSTFA derivatized molecular weight of 268 Da. Bernard et al (2013) have identified 2OHBnOH and catechol in the

355   GP of the reaction of BnOH and OH radicals. In our study, catechol was observed only in the H_2O_2 system in the PP.

356   Additional peaks were observed, which their mass spectra are consistent with products bearing OH and/or COOH groups,

357   however, their structural identification could not be obtained due to lack of authentic standards and the complexity of the

358   interpretation of their mass spectra. BnAld was reported to undergo secondary reactions (Sankar et al., 2014) and may

359   play an important role as precursor for some oxygenated species observed in this study.

360   **Particle phase products.** One of the advantages of conducting experiments in SS mode is collecting sufficient gas and

361   aerosol masses on denuders and filters for qualitative and quantitative offline analysis. In this study, aerosol collected on

362   GF filters were solvent extracted, with the resulting extracts subjected to BSTFA derivatization followed by GC-MS

363   analysis. SOA generated from both NOx and H_2O_2 systems was dominated by oxygenated organic compounds, for which

364   mass spectra for more than 50 species have been recorded. These species may have undergone several generations of

365   atmospheric oxidation. Several individual large peaks have been detected in addition to a significant number of small

366   peaks as shown in Figure 2. Figure 2 shows portions between 9 and 28 min of the TIC chromatograms of the silylated

367   derivatives of the aerosol extracts associated with BnOH/NOx (top) and BnOH/H_2O_2 (bottom). The portion after 28 min

368   is discussed in the next section. The chromatograms in Figure 2 can be directly compared because the chamber air sampled

369   and the amount of extract analyzed for each system were the same. This evaluation revealed that more than 70% of peaks

370   eluted from each system are identical, suggesting similar chemistry is involved in BnOH reaction products formed in the

371   presence and absence of NOx. In addition, a series of peaks dominated by fragments with odd m/z were observed only in

372   BnOH/NOx and their mass spectra were associated with nitrogen containing compounds as discussed in the NACs section

373   below. This suggests that the composition of a portion of SOA produced in the presence of NOx is different than that

374   formed in the absence of NOx, which can be clearly illustrated by the filters and extracts color shown in Figure 2 (bottom).

375   Consistent with the presence of nitroaromatics, filter F2 and methanol extract (E2) has lost most of the color seen in F1

376   and E1. The presence of NOx in the system produced material (filter F1) of a deep brown color. Most species structurally

377   identified in this study have not been reported in the literature, and mass spectra associated with several peaks are provided

378   either in the main manuscript or in the SI. Additional reaction products (e.g., oligomers, organonitrates) might have been

379   present in the SOA but could not be detected based on the analytical techniques used in this study. Note that formulae, in

380   particular chemical structure, could not be obtained for several peaks recorded in this study due to challenges interpreting

381 their mass spectra. A set of compounds identified and detected before 28 min in the present study are summarized in

382 Table 5.

383 Ring retaining products (e.g., 2-hydroxy benzyl alcohol, benzoic acid, 4-hydroxy benzoic acid, and catechol) were

384 detected in the PP in both systems. As noted above, some ring-retaining products were detected also in the GP as shown

385 in Table 5. Salicylaldehyde and 3-hydroxybenzaldehyde were present only in the GP. These two hydroxy-aldehydes may

386 undergo additional secondary reactions leading to some ring-opening products observed in this study. Representative EI

387 mass spectra of the TMS-derivatives associated with four compounds are shown in figure 3 including benzoic acid,

388 benzene-1,2-diol (catechol), 4-hydroxybenzoic acid, and 2-hydroxybenzyl alcohol. Additional EI and CI mass spectra are

389 shown in figures S4 and S5 in the SI. The EI mass spectrum of the BSTFA derivative of 2-hydroxybenzyl alcohol

390 displayed in figure 3 shows abundant fragment ions at m/z 73, 147, 267 ($M^{+\cdot}$), 253 ($M^{+\cdot} - 15$), and 179 ($M^{+\cdot} - 89$), and

391 weak ions at m/z 91, 223 and 163. The corresponding CI mass spectrum displayed in figure S4d shows abundant fragment

392 ions at m/z 268 ($M^{+\cdot}$), 253 ($M^{+\cdot} - 15$), and 179 ($M^{+\cdot} - 89$) and adduct ions at m/z 293 ($M^{+\cdot} + 29$) and 309 ($M^{+\cdot} + 41$). This

393 fragmentation pattern is consistent with the presence of a compound with two hydroxyl groups and a benzene ring (m/z

394 91) having molecular weight 268 for the BSTFA derivative, and MW 124 for its underivatized form. Similarly, the BSTFA

395 EI mass spectrum of 4-hydroxybenzoic acid (Figure 3c) shows characteristic fragment ions at m/z 73, 193 ($M^{+\cdot} - 89$), 223

396 ($M^{+\cdot} - 60$), 267 ($M^{+\cdot} - 15$) and 282 ($M^{+\cdot}$), and its CI mass spectrum fragment ions at m/z 73, 193, 67 and adducts at 283,

397 and 311. Again, these fragments and adducts are consistent with the presence of two (-OH) groups and a molecular weight

398 of the derivatized compound of 282 and 138 for the underivatized compound. The presence of a peak at m/z 153 ($M^{+\cdot} -$

399 117) is consistent with a compound bearing an organic acid group. The EI mass spectra recorded in this study for 2-

400 hydroxybenzyl alcohol and 4-hydroxybenzoic acid are identical to the reference NIST spectrum (webook.nist.gov). Figure

401 S5 shows EI mass spectra associated with four peaks eluted at 12.86, 15.58, 16.24, and 19.78 min consistent with the

402 fragmentation pattern of BSTFA derivatives, although their structures could not be obtained.

403 **Highly oxygenated compounds (HOCs).** Recent studies show that highly oxygenated compounds (e.g., HOMs) play an

404 important role in understanding SOA formation (Berndt et al. 2016, Jaoui et al., 2019; 2021 and references therein, Piletic

405 and Kleindienst, 2022). These compounds may result from several generations of atmospheric oxidation. In this study,

406 several ring-opening products eluted late in the chromatograms (RT > 25 min), with a relatively high O:C ratio of > 1.3

407 likely contributes to their condensation in the PP, were detected. Three groups of these oxidation products were detected

408 in the PP in both systems. Figure 4 shows the portion between 25 and 34 min of selected GC-MS extracted-ion

409 chromatograms where these groups (color coded) elute and uses the selected ions m/z 423, 437, and 525 (merged in one

410 chromatogram) to best illustrate them: (a) BnOH/NOx; (b) BnOH/H_2O_2; (c) chamber background. Groups 1, 2, and 3

411 consist of three (green), eight (blue) and four (red) peaks, respectively, and are completely absent from the background

412 chromatogram (figure 4c). Results from a comprehensive interpretation of EI and CI mass spectra associated with peaks

413 shown in figure 4 enabled the identification of several isomers associated with each group. Figure 5 displays three EI

414 mass spectra associated with each group main peak, along with proposed structure and chemical formulae. Table 6 gives

415 the major highly oxygenated compounds identified in this research, including the main peaks from each of these groups,

416 in the order of their underivatized molecular weight. Table 6 gives the chemical formulas, O:C mass ratio, the five most

417 abundant ions associated with each TMS derivative in methane-CI and EI modes, the molecular weights of the

418 underivatized (MW) and TMS-derivatized compounds (MW$_{BSTFA}$), and the proposed chemical structures of the

419 compounds.

420   Group 1 consists of *meso*-tartaric acid (*m*TA) (Rt 26.04 min), and *L*-/*D*-tartaric acids (*l*TA/*d*TA) (Rt 27.66 min)

421 identified based on authentic standards. The mass spectra of BSTFA derivatives of *l*TA and *d*TA standards (Figure S6,

422 SI) are very similar (eluting at the same time) and are only slightly different from the *m*TA (Figure S6: SI); however,

423 *l*TA/*d*TA and *m*TA elute at two different retention times (Figure 4, S6). The peak associated with *m*TA, and *l*TA/*d*TA are

424 among the largest peak observed in this portion of the chromatograms. Note, *l*TA isomer is the most abundant tartaric

425 acid present in nature (DeBolt et al., 2006). The fragments and adducts observed for the peak eluting at 25.19 min are

426 similar to those of mTA and d-/lTA and are consistent with the presence of four OH groups, a MW of 452 for the

427 derivatized compound and 164 for the underivatized compound, and a $C_4H_6O_6$ chemical formula. Tartaric acid has been

428 reported in ambient aerosol (Rohrl and Lammel, 2002; Gowda et al., 2016) and in chamber 1,3-butadiene SOA (Jaoui et

429 al., 2014). Recent studies suggest that tartaric acid and other hydroxy carboxylic acids undergo heterogeneous OH reaction

430 in aqueous solution, with the presence and position of OH group(s) playing an important role in fragmentation and

431 functionalization of organic aerosol (Cheng et al., 2016).

432   Group 2 consists of eight peaks (figure 4: blue) eluting between 28.5 and 31.5 min. The EI and CI mass spectra

433 associated with each peak display similar fragment and adduct ions across the range of 50 to 600 Da. The interpretation

434 of these mass spectra allows us to infer the molecular weight (MW) of the underivatized compounds as 164 and MW$_{BSTFA}$

435 of 452 for the TMS derivatives. The BSTFA CI mass spectrum of the peak eluted at 29.48 (largest peak) shows

436 characteristic fragment ions at m/z 73, 437 [$M^{+\cdot}$ -15], 363 [$M^{+\cdot}$ - 89], and 305 [$M^{+\cdot}$ - 105], and an adduct at 453 [$M^{+\cdot}$ + 1],

437 481 [$M^{+\cdot}$ + 29], and 493 [$M^{+\cdot}$ + 41]. These fragments and adducts are consistent with the presence of four OH groups and

438 an MW of 452 for the derivatized compound and 164 for the underivatized compound. The presence of peaks at m/z 347

439 [$M^{+\cdot}$ - 105], and 335 ($M^{+\cdot}$ – 117) are consistent with a compound bearing alcoholic and carboxylic OH groups

440 simultaneously. This mass spectrum is similar to the one from methyltartaric acid reported previously from isoprene

441 oxidation by our group (Jaoui et al., 2019). The silylated methyltartaric acid mass spectrum (Jaoui et al., 2019) and mass

442 spectra associated with group 2 are only slightly different, however, they elute at different retention times. The peaks have

443 been tentatively identified as isomers of trihydroxy-oxo-pentanoic acid, with the structure of 4-oxo-D-arabonic acid

444 isomer shown in Table 6.

445   Group 3 consists of four peaks eluting between 32.5 and 34 min (figure 4: red). The EI and CI mass spectra associated

446 with each peak display similar fragment and adduct ions across the range of 50 to 600 Da. As a descriptive example, an

447 EI mass spectrum is shown in Figure 5 for peak eluted at 33.1 min. A comprehensive interpretation of EI and CI mass

448 spectra associated with group 3 peaks (Figures 4, 5), allows us to infer the molecular weight (MW) of the underivatized

449 compounds as 180, and MW_{BSTFA} of 540 for the TMS derivatives, with a chemical formulae $C_5H_8O_7$. The compounds

450 corresponding to these four peaks were identified as isomers of C_5-trihydroxydicarboxylic acids. This identification is

451 tentative due to the absence of authentic standards, except for peak eluting at 33.47, which was identified as pentaric acid

452 (Table 6) based on authentic standard. The spectra of BSTFA derivatives of the remaining three red peaks are only slightly

453 different from the pentaric acid spectrum (Figure 6); however, they elute at different retention times. The EI mass spectra

454 are also similar to those reported in the literature for a set of C5-aldaric acids-TMS derivatives including xylaric, arabinaric

455 and ribaric acids (Hinton et al., 2008; https://pubchem.ncbi.nlm.nih.gov). Figure 6 shows the structure of pentaric acid

456 and its four isomers (a), the spectra associated with BSTFA derivative of pentaric acid observed in BnOH SOA (b: EI

457 mode), (c: CI-CH_4 mode), and standard (d: EI mode). Figure 6 also shows the structure of the main fragments observed

458 in BSTFA derivative of pentaric acid in EI mode including m/z at 540, 525, 407, 292, 147, and 73 Da. Pentaric acid and

459 its isomers (aldaric acids) are reported to be formed from the oxidation of aldopentose (Hinton, 2008; Derrien et al., 2018),

460 but no evidence has been provided for its presence in SOA samples. In the present study, we successfully identified aldaric

461 acids from the oxidation of BnOH in SOA samples.

462

463 **Nitroaromatic compounds (NACs).** NACs of secondary origin are a possible contributor to urban OA and not only

464 adversely affect human health and the environment but impact the aerosol optical properties and the atmospheric radiation

465 balance. By understanding the sources of NACs in ambient particles and their chemical identities, we can evaluate their

466 impact on the climate, environment, and human health. Recently, the analytical capabilities associated with BSTFA

467 derivatization have been extended to NACs bearing hydroxyl and carboxylic acid groups (Jaoui et al., 2018). Mass spectra

468 of most silylated NACs, especially methane-CI, are highly specific, reproducible, and produce characteristic fragments

469 useful in determining structural information and molecular weight, when authentic standards are not available (Jaoui et

470 al., 2018). In this study, a detailed analysis of mass spectra associated with peaks in chromatograms Figure 1c (GP) and

471 Figure 2 top (PP) reveals the presence of several peaks presenting similar fragmentation patterns as those reported by

472 Jaoui et al. (2018) for species bearing hydroxyl, carboxylic, nitro groups, and benzene ring. Figure 7 shows the portion

473 between 23 and 42 min of two +EI extracted ion chromatograms for the BSTFA derivatives at m/z 210, 165 (IS), 299 (IS),

474 300, 298, 372, 388 (merged in one chromatogram) associated with BnOH/NOx (top) and BnOH/H_2O_2 (bottom). The EI

475 and/or CI mass spectra of selected nitroaromatic standards can be found in Jaoui et al. (2018), and additional representative

476 subset of the derivatives are displayed in Figures S7 (SI). For clarity, figure 7 inset shows an expanded portion of the top

477 chromatogram between 26.7 – 28 min. Table 7 contains proposed identification of NACs detected in this study, along

478 with molecular weights, formulae, main 5 intense ions associated with CI and EI mass spectra of the derivatives, proposed

479 structure, and the GP to PP peak area ratio.

480   NACs with the highest confidence assignment are those identified by comparing their retention times, EI, and CI

481 mass spectra with those of reference standards, and NACs with low levels of confidence are those (1) that have been

482 identified previously in ambient PM or in smog chamber studies, (2) their EI mass spectra exist in the literature, or (3)

483 their molecular weights and numbers of OH, COOH, and NO_2 groups are simply consistent with the CI and EI mass

484 spectrum (Jaoui et al., 2018). A total of fourteen peaks associated with NACs were detected in this study. 3-Nitrobenzyl

485 alcohol, 4-nitrocatechol, 2-hydroxy-5-nitro benzyl alcohol, and 2-nitrophloroglucinol were identified based on authentic

486 standards. Three peaks eluted at 33.76, 34.70, and 34.76 having similar mass spectra as 2-nitrophloroglucinol (main peak)

487 eluted at 35.62 min were detected. They were tentatively associated with homologous series of 2-nitrophloroglucinol

488 including 3-nitrobenzene-1,2,4-triol, 5-nitropyrogallol, and 4-nitro-1,2,3-benzenetriol (not shown in Table 7). Similarly,

489 three additional peaks having similar mass spectra as 2-hydroxy-5-nitrobenzyl alcohol were observed and were tentatively

490 associated with homologous series of 2-hydroxy-5-nitrobenzyl alcohol including 4-hydroxy-2-nitrobenzyl alcohol. The

491   EIC in figure 7 (top) includes a series of four peaks observed only in the PP eluting at 35.94, 36.60, 38.18 min, whose

492   mass spectra were consistent with the presence of molecular weight 185 and 401 for the underivatized and derivatized

493   compounds, respectively. Based on similarity of their mass spectra, they were tentatively identified as structural

494   homologue of 3,4-dihydroxy-5-nitrobenzyl alcohol (Table 7) with $C_7H_7NO_5$ formulae. As can be seen in figure 7 (bottom),

495   NACs peaks were not detected in BnOH/H_2O_2 SOA extract, consistent with the formation of NACs in the presence of

496   NOx. All NACs were detected in both GPs and PP (Table 7), except 2-nitrophloroglucinol and 3,4-dihydroxy-5-

497   nitrobenzyl alcohol and their isomers were observed only in the PP consistent with their low volatility. This result suggests

498   that NACs may be formed in the GP, and partition to the PP for those with low volatility, although PP reactions may

499   occur as suggested by Charan et al. (2020) who analyzed only PP. 4-Nitrocatechol and 2-nitrophloroglucinol were among

500   the largest NAC peaks observed in our study (Figure 7). All three experiments conducted in this study were analyzed for

501   NACs to probe reproducibility of the BSTFA method and showed consistent results. 2-Nitrophloroglycinol, 4-

502   nitrocatechol and other NACs has been reported in PM collected in Pico Mountain Observatory, Pico Island in the Azores

503   archipelago by Ikemori et al., (2019). A series of NACs have been reported recently by Charan et al. (2020) in BnOH

504   SOA using off-line UPLC/ESIQ-ToFMS (ultra-high-performance liquid chromatography electrospray ionization

505   quadruple time of flight mass spectrometry), and the structure assigned to formulas obtained from MassLynk software

506   was based on expected oxidation products and MS/MS analysis. These observations support the identification of NACs

507   reported in this study. 4-Nitrophenol was reported in the GP by Bernard et al., (2013) at low yield and by Charan et al.

508   2020 in SOA from the OH radical oxidation of BnOH but was not detected either in the GP or the PP in this study.

509

510   **3.3. Mechanism of product formation**

511   Based on known GP reactions for aromatic compounds, a schematic representation for the reaction of BnOH with OH is

512   presented in schemes 1-3. It is developed to understand the chemistry leading to the main GP and PP products identified

513   experimentally in this study including HOCs and NACs. These schemes incorporate the latest experimental, quantum and

514   kinetic developments of the fate of peroxy/alkoxy benzoyl radicals including autooxidation (Wang, 2015; Sankar et al.

515   2014, and Namysl et al. 2020). The lines shown in these schemes are either one step or multistep pathways. Rate constants

516   at room temperature of BnOH with OH radical, O_3, and NO_3 radical of 2.8 10^{-11}, 6 x 10^{-19} (upper limit), and 4.0 x 10^{-15}

517   cm^3 molecule^{-1} s^{-1}, respectively, have been reported in the literature (Harrison and Wells, 2009, 2012; Bernard et al.,

518   2013). This suggests that the day-time oxidation of BnOH will be mainly initiated by OH radicals. The reaction for O_3

519 and NO$_3$ radical are not included in schemes 1-3, although they are expected to be formed as minor products in our

520 systems. Ozone is known to react primarily with compounds having double bonds and certainly not aromatic compounds.

521 Ozone concentrations are low and given in Table 2. Likewise, the NO$_3$ reaction with aromatic compounds tends to be

522 very slow and unlikely to have any impact in these systems. Moreover, given the O$_3$ + NO$_2$ reaction which gives NO$_3$

523 would only react with BnOH to a negligible degree.

524 The reaction of BnOH with OH radicals is initiated primarily by H atom abstraction from the external CH$_2$ group

525 leading to BnAld, and OH addition to the aromatic *ipso* (C1) and *ortho* (C2 or C6) positions to form two

526 alkyldihydroxyadducts R1 and R2 (scheme 1). The OH addition to the *para* (C3, C5) and *meta* (C4) position was reported

527 to be not favourable based on theoretical study of Wang, (2015). Scheme 1 shows mechanistic pathways leading to the
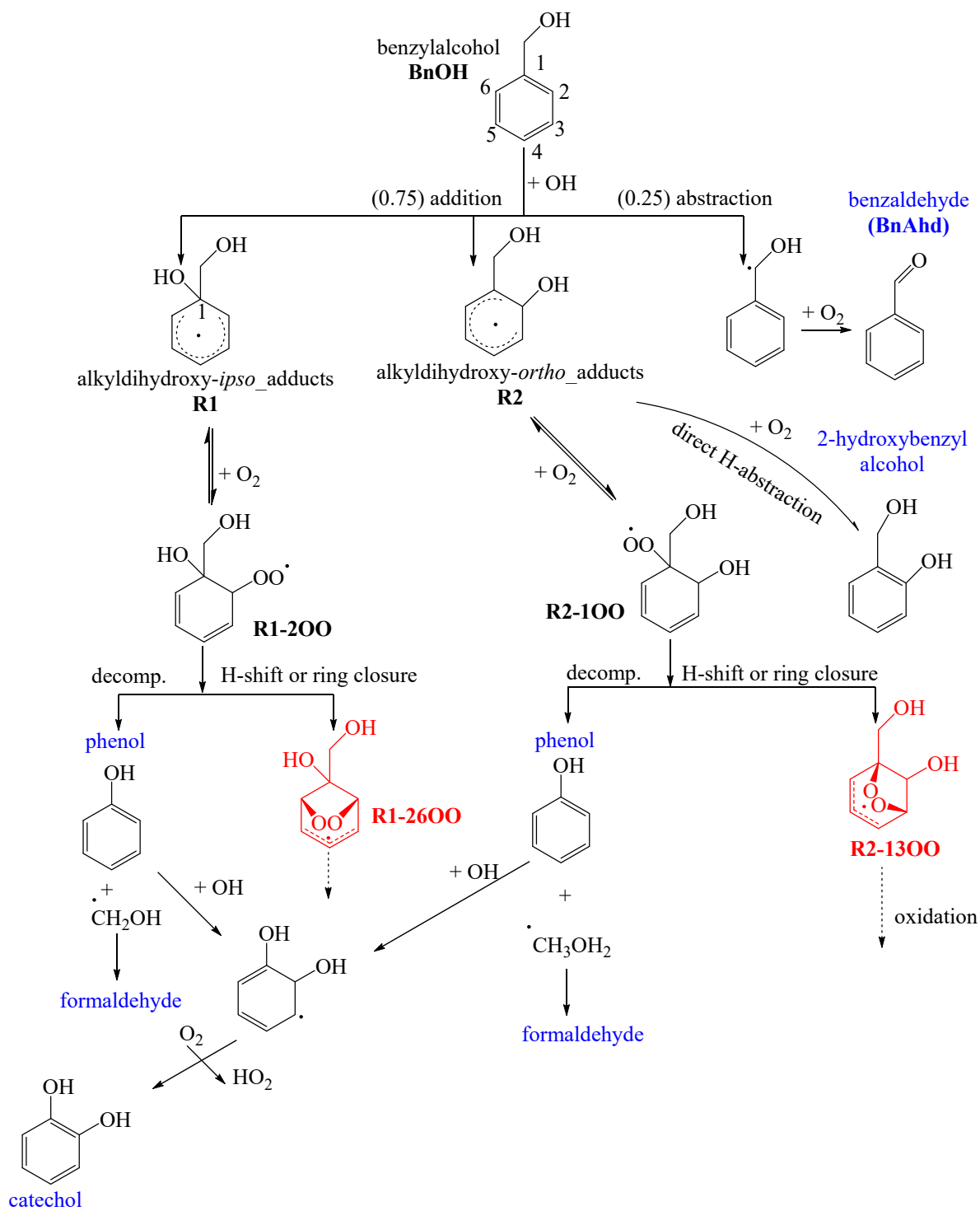
Scheme 1. Initial reaction pathways proposed to produce selected products detected in this study (blue color) in the gas or PP (Table 5). R1-26OO and R2-13OO intermediates undergo further reactions leading to ring-opening products as shown in scheme 3.

533 formation of stable products (blue) including BnAld, 4-hydroxybenzyl alcohol, 2-hydroxybenzyl alcohol, phenol,

534 formaldehyde, and catechol. The initial branching ratios shown in scheme 1 are those reported by Wang (2015), obtained

535 by combining quantum chemistry calculations and experimental work from the literature. BnAld was observed in this

536 study in the presence and absence of NOx, and its secondary chemistry may lead in part to oxygenated compounds

537 observed in this study (Bernard et al., 2013). Due to large number of possible intermediates formed (Wang, 2015), only

538 selected pathways energetically favourable leading to some products observed in this study are considered. We refer the

539 readers to Wang (2015) paper for an in-depth theoretical analysis of mechanistic pathways leading to the formation of

540 selected reaction products. The adduct R1 reacts rapidly through addition of O_2 to the ortho (C2) to produce peroxy

541 radicals R1-2OO, The O_2 addition to para position (C4) leading to R1-4OO peroxy radicals (not shown in Scheme 1) was

542 found to be endothermic, therefore negligible (Wang, 2015). Radicals R1-2OO undergo intramolecular H-shifts or ring

543 closures to form a stable bicyclic intermediate R1-26OO (red). Similarly, R2 reacts rapidly with O_2 to form peroxy radical

544 R2-1OO intermediate, which itself undergoes intramolecular H-shifts or ring closures to form a stable bicyclic

545 intermediate R2-13OO (red). R1-26OO and R2-13OO intermediates undergo further reactions leading to ring-opening

546 products as shown in scheme 3 below. 2-Hydroxybenzyl alcohol was proposed by Wang (2015) to form through the

547 reaction of R2 with O_2 involving rapid direct H-abstraction. A possible formation pathway of phenol is decomposition of

548 the peroxy radicals R1-2OO and R2-1OO through CH_2OH radical elimination (Bernard et al., 2013). As in Wang (2015),

549 the reverse reaction that gives R1 + O_2 is certainly competitive with the cyclization. Moreover, this reversible reaction

550 sustains the concentration of R1 with the radical now delocalized within the aromatic structure rather than associated with

551 the substituent O_2. By this approach, reactions of R1 lead to the formation of phenol and subsequent formation of catechol

552 as shown in Scheme 1. However, we do not have quantitative product data that would give insight to the R1-2OO and

553 R2-1OO decomposition (reverse) rate with respect to the O_2-cyclization rate. Note that the R1 reaction to form the phenol

554 is independent of NO_2 whereas the reaction of R1 to form nitrobenzyl alcohol is dependent on NO_2.

555 CH_2OH radical reacts rapidly with O_2 to produce formaldehyde. Catechol was proposed to originate from the reaction of

556 OH radicals with phenol (Atkinson et al., 1992) and with 2-hydroxybenzyl alcohol (Bernard et al., 20013).

557 NACs observed in this study (Table 7) are expected to be formed through reaction of OH radicals with BnOH in the

558 presence of NO_2. Scheme 2 briefly summarizes the main mechanistic pathways leading to BnOH NACs, which follow

559 similar chemistry as those reported for toluene, benzene, and xylenes (Jenkin et al., 2003; Vidovic et al., 2018) and

560 summarized by Wang et al., (2019). The steps shown in scheme 2 are multi-steps and the reader should consult the

561 reference papers above for more in depth information. NACs are proposed to originate from secondary reactions of

562 catechol, 1,3,5-trihydroxy benzene, and 4-hydroxybenzyl alcohol with OH radicals in the presence of NO2 (scheme 2).

563 These intermediates are proposed to be originated from R1, R2, and R3 adducts. Additional pathways could be initiated

564 via less well understood aqueous-phase nitration (Kroflic et al., 2018). 4-Nitrocatechol is proposed to be initiated through

565 the reaction of catechol with OH radicals in the presence of NOx (Finewax et al., 2018). 4-Hydroxy-2-nitrobenzyl alcohol

566 is proposed to be likely originated from the alkyldihydroxy-para-adduct formed from the OH addition to para position

567 (scheme 2). 2-Nitrophloroglucinol and 3,4-dihydroxy-5-nitrobenzyl alcohol follow similar reactions involving R3 adduct,

568 OH radicals, and NO_2.

569 According to Wang (2015) calculation, at high NO_2 (100 ppbv) the reaction of R1 with NO_2 can compete to a minor

570 degree with the reaction with O_2, therefore R1 possibly forms minor amounts of nitrobenzyl alcohol. This is similar to

571 that of other alkylbenzenes, such as toluene, although at much higher NO_2 concentrations (Wang, 2015). According to

572 the Wang calculation at 100 ppb NO_2, up to 30% of the R1 radical can form nitrobenzyl alcohol (unspecified nitro location

573 on the ring). When including the R2 radical which forms negligible levels of nitrobenzyl alcohol, no more than 20% (and

574 likely much less under our conditions) of the initial ring retaining radical would form nitrobenzyl alcohol. As noted in the

575 caption to table 1, the initial NOx is 98% NO and thus there is an extremely low initial concentration of NO_2. As the

576 extent of reaction increases, the NOy concentration increases as do other more oxidized forms of NOx. Thus, the addition

577 of NO_2 (~100 ppb) to the carbon-centered radical on the ring is of the same order as that described by Wang (2015) as

578 being of minor importance compared to O_2 addition. Thus, even though NOy concentrations in these experiments are

579 higher than ambient concentrations, we consider the findings and mechanisms of Wang (2015) to be relevant to this work.

580 We only have an upper limit to the NO_2 concentration, that is, NOy-NO. NOy represents in the NOx-NO from the oxides

581 of nitrogen (NOx) monitor. It is well known that the NOx monitor in the NOx-NO channel measures other oxidized

582 organic compounds in addition to NO_2.

583
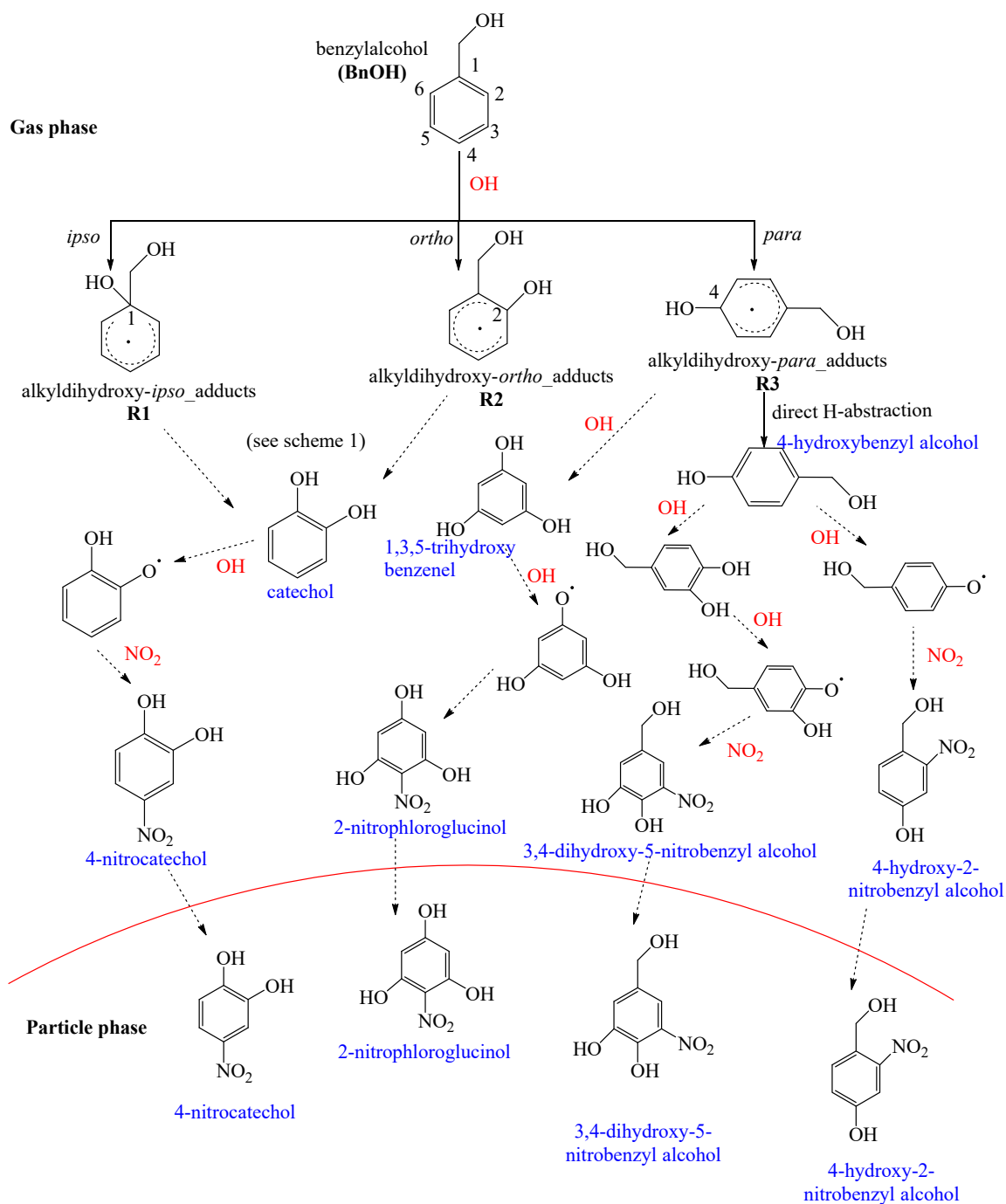
Scheme 2. Proposed mechanism for selected NAC species observed in this study.

HOCs were detected in the PP from the oxidation of BnOH in both low and high NOx systems (Table 6). Mechanistic pathways based on theoretical studies leading to several HOCs (e. g. HOMs) from the atmospheric oxidation of biogenic and aromatic hydrocarbons have been reported recently in the literature involving unimolecular reaction through

591 autoxidation, and peroxy and/or alkoxy radical isomerization (Wang, 2015; Jaoui et al., 2021; Piletic and Kleindienst,

592 2022). The formation of selected HOCs observed in this study is consistent with the following pathways proposed in

593 scheme 3 involving R2-1300 radical as the starting material. R1-26OO adduct undergoes similar reactions leading to

594 butenedial and 2,3-epoxy-butanedial as shown in scheme S1 (SI). Tartaric acid, 2,3,5-trihydroxy-4-oxo-pentanoic acid,

595 and pentaric acid, observed in this study for the first time, are proposed to be initiated by the oxidation of butenedial/2,3-

596 epoxy-butanedial, 5-hydroxy-4-oxo-2-penatenal, and 4-hydroxy-2,3-epoxypentandial (scheme 3). The mechanism
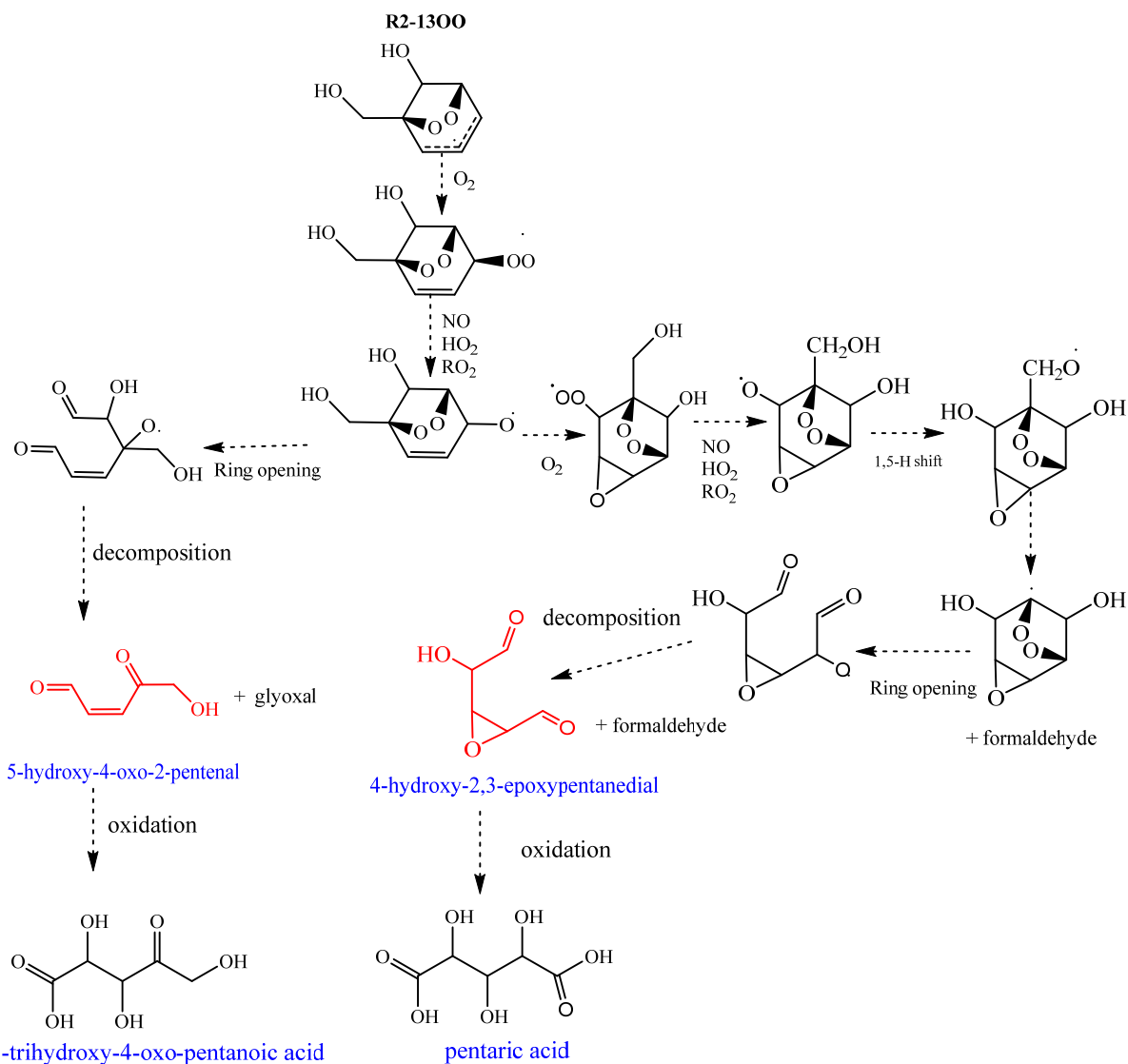
597 **Scheme 3.** Proposed mechanism for selected highly oxygenated compounds observed in this study.

598

599

600 leading to butenedial/2,3-epoxybutanal, 5-hydroxy-4-oxo-2-penatanal (scheme S1) was reported by Wang (2015) from

601 the OH oxidation of BnOH, therefore is not shown in scheme 3. Tartaric acid present in the PP at high level (Figure 4), is

602 proposed to be formed through the oxidation of butenedial and/or 2,3-epoxybutanal through classical oxidation of

603 aldehydes and alkenes to carboxylic acid (not shown in scheme 3). Similarly, 2,3,5-trihydroxy-4-oxo-pentanoic acid and

604 pentaric acid are proposed to rise from the oxidation of 5-hydroxy-4-oxo-2-pentenal, and 4-hydroxy-2,3-

605 epoxypentanedial, respectively following similar mechanistic pathways reported by Jaoui et al. (2021) for the formation

606 of methyltartaric acid from 4-hydroxy-2-methyl-but-2-enal involving peroxy and alkoxy radical isomerization (not

607 reported here). In this study, a new mechanism is proposed in scheme 3 leading to the formation of 4-hydroxy-2,3-

608 epoxypentanedial, which is the starting material for pentaric acid formation. It involves several intermediate steps

609 including unimolecular H migration (e.g., 1,5-H shift), ring opening and decomposition. Formaldehyde and glyoxal

610 observed in this study are also shown in scheme 3. The data used to support the secondary reactions of R2-13OO is

611 primarily product data shown in Scheme 3 which shows fragmentation products from R2-13OO. These products have

612 been well known for alkylbenzenes for many years. We have used analogous pathways for these alkylbenzenes to provide

613 an understanding as to how observed fragmentation products of BnOH are formed. However, it is important to note that

614 these fragmentation pathways follow from the formation of alkoxy radicals and not peroxy radicals. Thus, NO is required

615 in the system. (Note: $RO_2 + RO_2 \rightarrow 2RO + O_2$ is too slow to provide the alkoxy radicals needed for the fragmentation

616 reaction to occur.) Similar pathways are also applicable for R1-26OO.

617

618 **4. Summary**

619   In the present manuscript, laboratory experiments were conducted to investigate SOA formation from the oxidation

620 of benzyl alcohol in the presence and absence of NO_x. Chamber aerosol collected under these conditions has been

621 analyzed for organic mass to organic carbon ratio, and aerosol yield. In addition, the chemical composition of the gas

622 phase and SOA was analyzed using derivative-based methods followed by gas chromatography-mass spectrometry and

623 high-performance liquid chromatography analysis of the derivative compounds. More than 50 oxygenated organic

624 compounds in the gas and particle phases were identified. While a detailed non-targeted analysis has been made, our

625 primary focus has been to examine highly oxygenated and nitroaromatic compounds. The major components include ring-

626 opening products with high oxygen to carbon ratio (e. g. malic acid, tartaric acid, arabic acid, 2,3,5-trihydroxy-4-oxo-

627 pentanoic acid, and pentaric acid) and ring-retaining products (e. g. benzaldehyde, benzoic acid, catechol, 3-nitrobenzyl

628 alcohol, 4-nitrocatechol, 2-hydroxy-5-nitrobenzyl alcohol, 2-nitrophloroglucidol, 5-(hydroxymethyl)- 3-nitro-1,2-benzyl

629 diol). The presence of some of these products in the gas and particle phases simultaneously provides evidence of their

630   gas/particle partitioning. These oxygenated oxidation products made dominant contributions to the SOA particle

631   composition in both low and high NOx systems. Yields, organic mass to organic carbon ratio, and proposed reaction

632   schemes for selected compounds are provided.

633   Finally, a set of reaction pathways are proposed that accounts for selected reaction products observed in this study

634   from BnOH photooxidation in the presence of OH radicals, including NACs and HOCs. The proposed mechanism is

635   based on (1) theoretical studies reported previously in the literature and (2) mechanisms associated with aromatics

636   oxidation (e.g., benzene, toluene, xylenes…). New pathways were proposed for the formation of newly observed highly

637   oxygenated compounds tartaric acid, 2,3,5-trihydroxy-4-oxopentanoic acid, and pentaric acid. Butenedial/2,3epoxy-

638   butandial, 5-hydroxy-4-oxo-2-pentenal, and 4-hydroxy-2,3-expoxypentanedial were proposed as the starting intermediate

639   species leading to these highly oxygenated compounds. While theoretical studies involving unimolecular reactions were

640   developed focusing mainly on ring-containing products (Wang, 2015, Piletic and Kleindienst, 2022), similar theoretical

641   investigations focusing on linear species (Jaoui et al., 2021) as HOCs reported in this study will help strengthen the

642   pathways proposed here.

643   The results of this study potentially have atmospheric implications for areas impacted by benzyl alcohol including

644   urban and indoor areas and contribute to understanding the formation of ambient SOA from oxygenated anthropogenic

645   precursors. Nitroaromatics are pollutants of concern due to their toxicity, light-absorption properties, and relatively long

646   residence times in the environment. HOCs may partition into pre-existing particles or be involved in new particle

647   formation.

648
649
650

651   *Data Availability.* The data used in this study can be found at: https://catalog.data. gov/dataset/epa-sciencehub. DOI:

652   10.23719/1527893.

653

654   *Competing interests.* The authors declare no competing financial interest.

655

656   *Disclaimer.* This work has been subjected to the U.S. Environmental Protection Agency's administrative review and

657   approved for publication. The views expressed in this article are those of the authors and do not necessarily represent the

658   views or policies of the U.S. Environmental Protection Agency. Mention of trade names does not constitute endorsement

659   or recommendation of a commercial product by U.S. EPA.

660   **References**

661   Abend, A. M., Chung, L., Bibart, R. T., Brooks, M., and McCollum, D. G.: Concerning the stability of benzyl alcohol:

662   formation of benzaldehyde dibenzyl acetal under aerobic conditions, J. Pharm. Biomed. Anal., 34, 5, 957-962,

663   doi:10.1016/j.jpba.2003.11.007, 2004.

664

665   Akherati, A., Cappa, C. D., Kleeman, M. J., Docherty, K. S., Jimenez, J. L., Griffith, S. M., Dusanter, S., Stevens, P. S.,

666   and Jathar, S. H.: Simulating secondary organic aerosol in a regional air quality model using the statistical oxidation

667   model - Part 3: Assessing the influence of semi-volatile and intermediate-volatility organic compounds and NOx, Atmos.

668   Chem. Phys., 19, 4561–4594, 2019.

669

670   Alton, M. W., and Browne, L. C.: Atmospheric chemistry of volatile methyl siloxanes: kinetics and products of oxidation

671   by OH radicals and Cl atoms, Environ. Sci. Technol., 54, 5992−5999, 2020.

672

673   Antonelli, L., Mapelli, E., Strini, A., Cerulli, T., Leoni, R., and Stella S.: Laboratory and real scale comparative study of

674   benzyl alcohol emission from a two-component epoxy paint, Proceedings: Indoor Air, 584-589, 2002.

675

676   Atkinson, R., Aschmann, S. M., and Arey, J.: Reactions of OH and N03 Radicals with Phenol, Cresols, and 2-Nitrophenol

677   at 296 ± 2 K, Environ. Sci. Technoi. 1992, 26, 1397-1403, 1992.

678

679   Bernard, B., Magneron, I., Eyglunent, G., Daële, V., Wallington, T. J., Hurley, M. D., and Mellouki, A.: Atmospheric

680   chemistry of benzyl alcohol: kinetics and mechanism of reaction with OH radicals, Environ. Sci. Technol., 47,

681   3182−3189, 2013.

682

683   Berndt, T., Herrmann, H., Sipila, M., and Kulmala, M.: Highly oxidized second-generation products from the gas-phase

684   reaction of OH radicals with isoprene. J. Phys. Chem. A, 120 (51), 10150− 10159, 2016.

685

686   Boatright, J., Negre, F., Chen, X., Kish, C. M., Wood, B., Peel, G., Orlova, I., Gang, D., Rhodes, D., and Dudareva, N.:

687   Understanding in vivo benzenoid metabolism in petunia petal tissue, Plant Physiol., 135, 1993−2011, 2004.

688

689   Carter, W. P. L., Malkina, I. L., Cocker III, D. R., and Song, C.: Environmental chamber studies of VOC species in

690   architectural coating and mobile source emissions, South Coast Air Quality Management District Contract No. 03468,

691   2005.

692

693   Charan, S. M., Buenconsejo, R. S., and Seinfeld, J. H.: Secondary organic aerosol yields from the oxidation of benzyl

694   alcohol, Atmos. Chem. Phys., 20, 13167–13190, doi:10.5194/acp-2020-49, 2020

695

696   Charan, S. M., Huang, Y., Buenconsejo, R. S., Li, Q., Cocker III, D. R., and Seinfeld, J. H.: Secondary organic aerosol

697   formation from the oxidation of decamethylcyclopentasiloxane at atmospherically relevant OH concentrations, Atmos.

698   Chem. Phys., 22, 917-928, doi:10.5194/acp-22-917-2022, 2021.

699

700   Cheng, C. T., Chan, M. N., and Wilson, K. R.: Importance of unimolecular HO2 elimination in the heterogeneous OH

701   reaction of highly oxygenated tartaric acid aerosol, J. Phys. Chem. A, 120, 5887−5896, doi: 10.1021/acs.jpca.6b05289,

702   2016.

703

704   Coggon, M. M., Gkatzelis, G. I., McDonald, B. C., Gilman, J. B., Schwantes, R. H., Abuhassan, N., Aikin, K. C., Arendd,

705   M. F., Berkoff, T. A., Brown, S. S., Campos, T. L., Dickerson, R. R., Gronoff, G., Hurley, J. F., Isaacman-VanWertz, G.,

706   Koss, A. R., Lia, M., McKeen, S. A., Mosharyd, F., Peischl, J., Pospisilova, V., Renh, X., Wilson, A., Wu, Y., Trainer,

707   M., and Warneke, C.: Volatile chemical product emissions enhance ozone and modulate urban chemistry,

708   doi:10.1073/pnas.2026653118, PNAS, 118, 32, e2026653118, 2021.

709

710   DeBolt, S., Cook, D. R., and Ford, C. M.: L-Tartaric acid synthesis from vitamin C in higher plants, PNAS, 103 (14) 5608-

711   5613, doi: 10.1073/pnas.0510864103, 2006.

712

713   Derrien, E., Ahmar, M., Martin-Sisteron, E., Raffin, G., Queneau, Y., Marion, P., Beyerle, M., Pinel, C., and Besson, M.:

714   Oxidation of aldoses contained in softwood hemicellulose acid hydrolysates into aldaric acids under alkaline or

715   noncontrolled pH conditions, Industrial & Engineering Chemistry Research, 57 (13), 4543-4552, doi.:

716   10.1021/acs.iecr.8b00239, 2018.

717

718   Do, J. Y., Salunkhe, D. K., and Olson, L. E.: Isolation, identification and comparison of the volatiles of peach fruit as

719   related to harvest maturity and artificial ripening, J. Food Sci., 34, 618−621, 1969.

720

721   Ferri, D., Mondelli, C., Krumeich, F., and Baiker, A.: Discrimination of active palladium sites in catalytic liquid-phase

722   oxidation of benzyl alcohol, J. Phys. Chem. B., 110, 46, 22982-22986, doi:10.1021/jp065779z, 2006.

723

724   Finewax, Z., de Gow, J. A., and Ziemann, P. J.: Identification and Quantification of 4-Nitrocatechol Formed from OH

725   and NO_3 Radical-Initiated Reactions of Catechol in Air in the Presence of NO_x: Implications for Secondary Organic

726   Aerosol Formation from Biomass Burning, Environmental Science & Technology, 52 (4), 1981-1989, doi.:

727   10.1021/acs.est.7b05864, 2018.

728

729   Fu, Zi., Xie, H., Elm, J., Guo, X., Fu, Zh., and Chen, J.: Formation of low-volatile products and unexpected high

730   formaldehyde yield from the atmospheric oxidation of methylsiloxanes, Environ. Sci. Technol., 54, 12, 7136-7145,

731   doi:10.1021/acs.est.0c01090, 2020.

732

733   Gkatzelis, G. I., Coggon, M. M., McDonald, B. C., Peischl, J., Aikin, K. C., Gilman, J. B., Trainer, M., and Warneke, C.:

734   Identifying volatile chemical product tracer compounds in U.S. Cities, Environ. Sci. Technol.,

735   doi:10.1021/acs.est.0c05467, 55, 188−199, 2021.

736

737   Gowda, D., Kawamura, K., and Tachibana, E.: Identification of hydroxy- and keto-dicarboxylic acids in remote marine

738   aerosols using gas chromatography/quadruple and time-of-flight mass spectrometry, Rapid Communications in Mass

739   Spectrometry, 30(7), 992–1000, doi: 10.1002/rcm.7527, 2016.

740

741   Harrison, J. C., and Wells, J. R.: Gas-phase chemistry of benzyl alcohol: reaction rate constants and products with OH

742   radical and ozone, Atmos. Environ., 43, 798−804, 2009.

743

744 Harrison, J. C., and Wells, J. R.: 2-Butoxyethanol and benzyl alcohol reactions with the nitrate radical: rate coefficients

745 and gas-phase products, Int. J. Chem. Kinet., 44, 778−788, 2012.

746

747 Hayes, P. L., Carlton, A. G., Baker, K. R., Ahmadov, R., Washenfelder, R. A., Alvarez, S., Rappenglück, B., Gilman, J.

748 B., Kuster, W. C., de Gouw, J. A., Zotter, P., Prévôt, A. S. H., Szidat, S., Kleindienst, T. E., Offenberg, J. H., Ma, P. K.,

749 and Jimenez, J. L.: Modeling the formation and aging of secondary organic aerosols in Los Angeles during CalNex 2010,

750 Atmos. Chem. Phys., 15, 5773–5801, 2015.

751

752 Hinton, M. R.: Xylaric acid, D-arabinaric acid (D-lyxaric acid), L-arabinaric acid (L-lyxaric acid), and Ribaric acid-1,4-

753 lactone; Synthesis and isolation-synthesis of polyhydroxypolyamides therefrom, Theses, Dissertations, & Professional

754 Papers. 1202, https://scholarworks.umt.edu/etd/1202, 2008.

755

756 Hodzic, A., Jimenez, J. L., Madronich, S., Aiken, A. C., Bessagnet, B., Curci, G., Fast, J., Lamarque, J.-F., Onasch, T.

757 B., Roux, G., Schauer, J. J., Stone, E. A., and Ulbrich, I. M.: Modeling organic aerosols during MILAGRO: importance

758 of biogenic secondary organic aerosols, Atmos. Chem. Phys., 9, 6949–6981, 2009.

759

760 Horvat, R. J., Chapman, G. W., Jr., Robertson, J. A., Meredith, F. I., Scorza, R., Callahan, A. M., and Morgens, P.:

761 Comparison of the volatile compounds from several commercial peach cultivars, J. Agric. Food Chem., 38, 234−237,

762 1990.

763

764 Humes, M. B., Wang, M., Kim, S., Machesky, J. E., Gentner, D. R., Robinson, A. L., Donahue, N. M., and Presto, A. A.:

765 Limited secondary organic aerosol production from acyclic oxygenated volatile chemical products, Environ. Sci. Technol.

766 56, 4806−4815, 2022.

767

768 Humpf, H. U., and Schreier, P.: Bound aroma compounds from the fruit and the leaves of blackberry (Rubus laciniata L.),

769 J. Agric. Food Chem., 39, 1830−1832, 1991.

770

771 Ikemori, E., Nakayama, T., and Hasegawa, H.: Characterization and possible sources of nitrated mono- and di-aromatic

772 hydrocarbons containing hydroxyl and/or carboxyl functional groups in ambient particles in Nagoya, Japan, Atmos.

773 Environ., 211, 91-102, 2019.

774

775 Janechek, N. J., Marek, R. F., Bryngelson, N., Singh, A., Bullard, R. L., Brune, W. H., and Stanier, C. O.: Physical

776 properties of secondary photochemical aerosol from OH oxidation of a cyclic siloxane, Atmos. Chem. Phys., 19, 1649–

777 1664, 2019.

778

779 Jaoui, M., and Kamens, R. M.: Mass balance of gaseous and particulate products analysis from α-pinene/NO_x/air in the

780 presence of natural sunlight, J. Geophys. Res., 106, D12, 12,541-12,558, doi:10.1029/2001JD900005, 2001.

781

782 Jaoui, M., Kleindienst, T. E., Lewandowski, M., and Edney, E. O.: Identification and quantification of aerosol polar

783 oxygenated compounds bearing carboxylic and/or hydroxyl groups, 1. Method development, Anal. Chem., 76, 4765–

784 4778, 2004.

785

786 Jaoui, M., Kleindienst, T. E., Lewandowski, M., Offenberg, J. H., and Edney, E. O.: Identification and quantification of

787 aerosol polar oxygenated compounds bearing carboxylic or hydroxyl groups. 2. Organic tracer compounds from

788 monoterpenes, Environ. Sci. Technol., 39, 5661–5673, 2005.

789

790 Jaoui, M., Kleindienst, T. E., Docherty, K. S., Lewandowski, M., and Offenberg, J. H.: Secondary organic aerosol

791 formation from the oxidation of a series of sesquiterpenes: a-cedrene, b-caryophyllene, a-humulene and a-farnesene with

792 O_3, OH and NO_3 radicals, Environ. Chem. 10, 178–193, doi:10.1071/EN13025, 2013.

793

794 Jaoui, M., Lewandowski, M., Docherty, K., Offenberg, J. H., and Kleindienst, T. E.: Atmospheric oxidation of 1,3-

795 butadiene: characterization of gas and aerosol reaction products and implications for $PM_{2.5}$, Atmos. Chem. Phys., 13681–

796 13704, doi: 10.5194/acp-14-1368114, 2014.

797

798   Jaoui, M., Lewandowski, M., Offenberg, H. J., Colon, M., Docherty, K. S., and Kleindienst, T. E: Characterization of

799   aerosol nitroaromatic compounds: Validation of an experimental method, Mass Spectrom., 53, 680–692, 2018.

800

801   Jaoui, M., Szmigielski, R., Nestorowicz, K., Kolodziejczyk, A., Sarang, K., Rudzinski, K. J., Konopka, A., Bulska, E,

802   Lewandowski, M., And Kleindienst, T. E.: Organic hydroxy acids as highly oxygenated molecular (HOM) tracers for

803   aged isoprene aerosol, Environmental Science & Technology, 53 (24), 14516-14527, doi: 10.1021/acs.est.9b05075, 2019.

804

805   Jaoui, M., Piletic, I., Szmigielski, R., Rudzinski, J. K., E, Lewandowski, M., Riedel, T. P., and Kleindienst, T. E.: Rapid

806   production of highly oxidized molecules in isoprene aerosol via peroxy and alkoxy radical isomerization pathways in low

807   and high NO_x environments: Combined laboratory, computational and field studies, Science of The Total Environment,

808   775, 145592, doi: 10.1016/j.scitotenv.2021.145592, 2021

809

810   Jenkin, M. E., Saunders, S. M., Wagner, V., and Pilling, M. J.: Protocol for the development of the Master Chemical

811   Mechanism, MCM v3 (Part B): tropospheric degradation of aromatic volatile organic compounds, Atmos. Chem. Phys.,

812   3, 181–193, https://doi.org/10.5194/acp-3-181-2003, 2003.

813

814   Khare, P., and Gentner, D. R.: Considering the future of anthropogenic gas-phase organic compound emissions and the

815   increasing influence of non-combustion sources on urban air quality, Atmos. Chem. Phys., 18, 5391–5413, 2018.

816

817   Kleindienst, T. E., Edney, E. O., Lewandowski, M., Offenberg, J. H., and Jaoui M.: Secondary organic carbon and aerosol

818   yields from the irradiations of isoprene and   -pinene in the presence of NO_x and SO_2, Environ. Sci. Technol., 40, 3807–

819   3812, 2006.

820

821   Kleindienst, T. E., Lewandowski, M., Offenberg, J. H., Jaoui, M., and Edney, E. O.: The formation of secondary organic

822   aerosol from the isoprene + OH reaction in the absence of NO_x, Atmos. Chem. Phys., 9, 6541–6558, 2009.

823

824   Kleindienst, T. E., Jaoui, M., Lewandowski, M., Offenberg, J. H., and Docherty, K. S.: The formation of SOA and

825   chemical tracer compounds from the photooxidation of naphthalene and its methyl analogs in the presence and absence

826   of nitrogen oxides, Atmos. Chem. Phys., doi:10.5194/acp-12-8711-2012, 12, 8711–8726, 2012.

827

828   Kroflic, A., Hus, M., Grilc, M., and Grgic, I.: Underappreciated and complex role of nitrous acid in aromatic nitration

829   under mild environmental conditions: the case of activated methoxyphenols, Environ. Sci. Technol., 52, 13756–13765,

830   https://doi.org/10.1021/acs.est.8b01903, 2018.

831

832   Kroll, J. H., Chan, A. W. H., Ng, N. L., Flagan, R. C., and Seinfeld, J. H.: Reactions of semivolatile organics and their

833   effects on secondary organic aerosol formation, Environ. Sci. Technol., 41, 3545–3550, 2007.

834

835   Larsen, M., and Poll, L.: Odor thresholds of some important aroma compounds in raspberries, Z. Lebensm. Unters. Forsch,

836   191, 129−131, 1990.

837

838   Lewandowski, M., Jaoui, M., Offenberg, J. H., Krug, J. D., and Kleindienst, T. E.: Atmospheric oxidation of isoprene and

839   1,3-butadiene: influence of aerosol acidity and relative humidity on secondary organic aerosol, Atmos. Chem. Phys., 15,

840   3773–3783, doi:10.5194/acp-15-3773-2015, 2015.

841

842   Li, W., Li, L., Chen, C-L, Kacarab, M., Peng, W., Price, D., Xu, J., and Cocker III, D. R.: Potential of select intermediate-

843   volatility organic compounds and consumer products for secondary organic aerosol and ozone formation under relevant

844   urban conditions, Atmos. Environ., 118, 109-117, 2018.

845

846   Lu, Q., Murphy, B. N., Momei Q., Adams, P. J., Zhao, Y., Pye, H. O. T., Efstathiou, C., Allen, C., and Robinson, A. L.:

847   Simulation of organic aerosol formation during the CalNex study: updated mobile emissions and secondary organic

848   aerosol parameterization for intermediate-volatility organic compounds, Atmos. Chem. Phys., 20, 4313–4332, 2020.

849

850   McDonald, B. C., De Gouw, J. A., Gilman, J. B., Jathar, S. H., Akherati, A., Cappa, C. D., Jimenez, J. L., Lee-Taylor, J.,

851   Hayes, P. L., McKeen, S. A., Cui, Y. Y., Kim, S. W., Gentner, D. R., Isaacman-VanWertz, G., Goldstein, A. H., Harley,

852 R. A., Frost, G. J., Roberts, J. M., Ryerson, T. B., and Trainer, M.: Volatile chemical products emerging as largest

853 petrochemical source of urban organic emissions, Science, 359, 760–764, 2018.

854

855 Milani, A., Al-Naiema, I. M., and Stone, E. A: Detection of a secondary organic aerosol tracer derived from personal care

856 products, Atmos. Environ., 246, 118078, 2021.

857

858 Mohr, C., DeCarlo, P. F., Heringa, M. F., Chirico, R., Richter, R., Crippa, M., Querol, X., Baltensperger, U., and Prévôt,

859 A. S. H.: Spatial variation of aerosol chemical composition and organic components identified by positive matrix

860 factorization in the Barcelona region, Environ. Sci. Technol., 49, 10421–10430, 2015.

861

862 Namysl, S., Pelucchi, M., Maffei, L. P., Herbinet, O., Stagni, A., Faravelli, T., and Battin-Leclerc, F.: Experimental and

863 modeling study of benzaldehyde oxidation, Combustion and Flame, 211, 124–132, 2020.

864

865 Offenberg, J. H., Lewandowski, M., Edney, E. O., Kleindienst, T. E., Jaoui, M.: Investigation of a systematic offset in the

866 measurement of organic carbon with a semicontinuous analyzer, J. A&WMA, 57:5, 596-599, doi:10.3155/1047-

867 3289.57.5.596, 2007

868

869 Orlova, I., Marshall-Colón, A., Schnepp, J., Wood, B., Varbanova, M., Fridman, E., Blakeslee, J. J., Peer, W. A., Murphy,

870 A. S., Rhodes, D., Pichersky, E., and Dudareva, N.: Reduction of Benzenoid synthesis in petunia flowers reveals multiple

871 pathways to benzoic acid and enhancement in auxin transport, Plant Cell, 18, 3458−3475, 2006.

872

873 Pennington, E. A., Seltzer, K. M., Murphy, B. N., Qin, M., Seinfeld, J. H., Pye, H. O. T.: Modeling secondary organic

874 aerosol formation from volatile chemical products, Atmos. Chem. Phys., doi:10.5194/acp-21-18247-18261-2021, 18247-

875 18261, 2021.

876

877 Piletic, I. R., and Kleindienst, T. E.: Rates and Yields of Unimolecular Reactions Producing Highly Oxidized Peroxy

878 Radicals in the OH-Induced Autoxidation of α-Pinene, β-Pinene, and Limonene, *The Journal of Physical Chemistry A.*

879 *126* (1), 88-100, doi: 10.1021/acs.jpca.1c07961, 2022.

880

881   Qin, M. M., Murphy, B. N., Isaacs, K. K., McDonald, B. C., Lu, Q. Y., McKeen, S. A., Koval, L., Robinson, A. L.,

882   Efstathiou, C., Allen, C., and Pye, H. O. T.: Criteria pollutant impacts of volatile chemical products informed by near-

883   field modelling, Nature Sustainability, 4, 129–137, https://doi.org/10.1038/s41893-020-00614-1, 2021.

884

885   Rohl, A., and Lammedl. G.: Determination of malic acid and other C4 dicarboxylic acids in atmospheric aerosol samples,

886   Chemosphere, 46(8), 1195-1199, doi: 10.1016/s0045-6535(01)00243-0, 2002.

887

888   Sankar, S., Nowicka, E., Carter, E., Murphy, D. M., Knight, D. W., Bethell, D., and Hutchings, G. J.: The benzaldehyde

889   oxidation paradox explained by the interception of peroxy radical by benzyl alcohol, Nature Communic,

890   doi:10.1038/ncomms4332, 5, 3332, 2014.

891

892   Seltzer, K. M., Murphy, B. N., Pennington, E. A., Allen, C., Talgo, K., and Pye, H. O. T.: Volatile chemical product

893   enhancements to criteria pollutants in the United States, Environ. Sci. technol., doi:10.1021/acs.est.1c04298, 2021.

894

895   Shilling, J. E., Chen, Q., King, S. M., Rosenoern, T., Kroll, J. H., Worsnop, D. R., McKinney, K. A., and Martin, S. T.:

896   Particle mass yield in secondary organic aerosol formed by the dark ozonolysis of α-pinene, Atmos. Chem. Phys., 8,

897   2073–2088, doi:10.5194/acp-8-2073-2008, 2008.

898

899   Smith, D. F., Kleindienst, T. E., and Hudgens, E. E.: Improved high-performance liquid chromatographic method for

900   artifact free measurements of aldehydes in the presence of ozone using 2,4-dinitrophenylhydrazine, J. Chromatogr. A,

901   483, 431–436, 1989.

902

903   Stockwell, C. E., Coggon, M. M., Gkatzelis, G. A., Ortega, J., McDonald, B. C., Peischl, J., Aikin, K., Gilman, J. B.,

904   Trainer, M., and Warneke, C.: Volatile organic compound emissions from solvent- and water borne coatings:

905   compositional differences and tracer compound identifications, Atmos. Chem. Phys., 21, 6005–6022, doi:10.5194/acp-

906   21-6005-2021, 2021.

907

908   Urakami, K., Kobayashi, C., Miyazaki, Y., Nishijima, K., and Yoshimura, Y.: Degradation products generated by

909   sonication of benzyl alcohol, a sample preparation solvent for the determination of residual solvents in pharmaceutical

910   bulks, on capillary gas chromatography, Chem. Pharm. Bull., 48, 1299–1303, 2000.

911

912   Vallat, A., and Dorn, S.: Changes in volatile emissions from apple trees and associated response of adult female codling

913   moths over the fruit-growing season, J. Agric. Food Chem., 53, 4083−4090, 2005.

914

915   Vidovic, K., Lasic Jurkovic, D., Sala, M., Kroflic, A., and Grgic, I.: Nighttime aqueous-phase formation of nitrocatechols

916   in the atmospheric condensed phase, Environ. Sci. Technol., 52, 9722– 9730, https://doi.org/10.1021/acs.est.8b01161,

917   2018.

918

919   Vlachou, A., Daellenbach, K. R., Bozzetti, C., Chazeau, B., Salazar, G. A., Szidat, S., Jaffrezo, J. L., Hueglin, C.,

920   Baltensperger, U., El Haddad, I., and Prévôt, A. S.: Advanced source apportionment of carbonaceous aerosols by coupling

921   offline AMS and radiocarbon size-segregated measurements over a nearly 2-year period. Atmos. Chem. Phys., 18, 6187–

922   6206, 2018.

923

924   Wang, L.: The atmospheric oxidation mechanism of benzyl alcohol initiated by OH radicals: the addition channels, Chem.

925   Phys. Chem., *16* (7), 1542-1550, doi:10.1002/cphc.201500012, 2015.

926

927   Wang, N., Jorga, S. D., Pierce, J. R., Donahue, N. M., and Pandis, S. N.: Particle wall-loss correction methods in smog

928   chamber experiments, Atmos. Meas. Tech., 11, 6577–6588, doi:10.5194/amt-11-6577-2018, 2018.

929

930   Wang, Y., Hu, M., Wang, Y., Zheng, J., Shang, D., Yang, Y., Liu, Y., Li, X., Tang, R., Zhu, W., Du, Z., Wu, Y., Guo, S.,

931   Wu, Z., Lou, S., Hallquist, M., and Yu, J. Z.: The formation of nitro-aromatic compounds under high NOx and

932   anthropogenic VOC conditions in urban Beijing, China, Atmos. Chem. Phys., 19, 7649–7665, 2019.

933

934   Weschler, C. J.: Chemistry in indoor environments: 20   years of research, Indoor Air, 21 (3), 205-218, 2011.

935

936   Wu, Y., and Johnston, M. V.: Molecular characterization of secondary aerosol from oxidation of cyclic methylsiloxanes,

937   J. Am. Soc. Mass. Spectr., 27, 402–409, doi:10.1007/s13361-015-1300-1, 2016.

938

939   Wu, Y., and Johnston, M. V.: Aerosol formation from OH oxidation of the volatile cyclic methyl siloxane (cVMS)

940   Decamethylcyclopentasiloxane, Environ. Sci. Technol., 51, 4445– 4451, doi:10.1021/acs.est.7b00655, 2017.

941

942   Zhao, B., Wang, S., Donahue, N. M., Jathar, S. H., Huang, X., Wu, W., Hao, J., and Robinson, A. L.: Quantifying the

943   effect of organic aerosol aging and intermediate volatility emissions on regional-scale aerosol pollution in China, Sci.

944   Rep., 6, 28815, doi:10.1038/srep28815, 2016.

945

946   Zhang, X., Cappa, C. D., Jathar, S. H., McVay, R. C., Ensberg, J. J., Kleeman, M. J., and Seinfeld, J. H.: Influence of

947   vapor wall loss in laboratory chambers on yields of secondary organic aerosol, PNAS, doi:10.1073/pnas.1404727111,

948   111 (16), 5802-5807, 2014.

949

950

951

952

953

954

955

956

957

958

959

960

961

962

963

964 **Table 1.** Initial conditions for BnOH experiments in the presence and absence of NO.

Exp. IDs	BnOH (ppb)	H_2O_2 (ppm)	NO[a] (ppb)	Seed surface area (nm^2 cm^{-3})	BnOH/NO (ppb/ppb)	T ($^{\circ}$C)	RH (%)
ER-889	385	-	178	4.67×10^7	2.2	24.5	31.0
ER-890	355	-	96	4.94×10^7	3.7	24.5	31.1
ER-891	723	-	188	9.88×10^7	3.8	24.6	31.3
ER-892	319	3.04	-	1.36×10^6	-	25.7	< 4.0

965 T: temperature; RH: relative humidity. Seed aerosol at 1 µg m^{-3}. [a]: The initial NOx during the irradiations was greater than 98% NO.

966

967 **Table 2.** Steady-state GP and reacted BnOH and NO concentration during the irradiations.

Exp. IDs	NO (ppb)	Reacted NO (ppb)	BnOH (ppb)	Reacted BnOH (ppb)	BnOH/NO ratio (ppb/ppb)	O_3 (ppb)	NOy (ppb)
ER889	78	100	132	253	1.7	30	163
ER890	9	87	132	223	14.7	147	80
ER891	29	159	387	336	13.4	11	146
ER892	-	-	85	234	-	28	-

968

969 **Table 3.** Formation and yields of SOA (Y_{SOA}) and SOC (Y_{SOC}). All organic and carbon aerosol masses are corrected for
970 a wall loss of 0.067 h^{-1} (Kleindienst et al., 2012).

Exp. IDs	SOA (µg/m^3)	SOC (µgC/m^3)	SOA/SOC	Y_{SOA} (%)	Y_{SOC} (%)
ER889	39.6	23.2	1.7	3.6	2.7
ER890	56.1	30.3	1.9	5.7	4.0
ER891	119.5	58.9	2.0	8.1	5.1
ER892	52.9	24.8	2.1	5.2	3.1

971
972
973
974
975
976
977
978
979
980
981

982 **Table 4.** Steady state carbonyl concentrations (ppmV) during BnOH oxidation (FH: formaldehyde; AH: acetaldehyde;

983 Ac: acetone; MA: methacrolein; BN: 2-butanone; BnAld: benzaldehyde; G: glyoxal; MG: methylglyoxal).

Exp. ID	FH	AH	Ac	MA	BN	BnAld	G	MG
ER889	2.4	1.2	1.0	1.0	0.6	23.09	5.0	0.6
ER890	1.5	2.8	-	-	2.9	18.2	3.8	0.4
ER891	5.1	2.5	1.3	2.0	1.4	30.8	8.6	0.6
ER892	181.7	23.5	-	0.8	0.8	5.2	7.8	1.6

984

985

986

987

988

989

990

991

992

993

994

995

996

997

998

999

1000

1001

1002
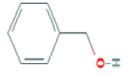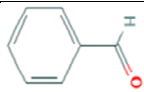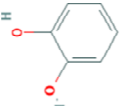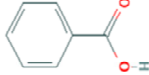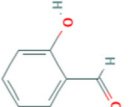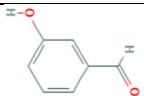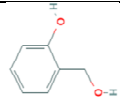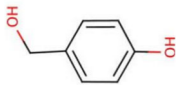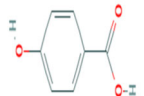
1003

1004

1005

1006 **Table 5.** Summary of selected reaction products detected and identified either in gas-phase (GP), particle phase (PP) or
1007 both from BnOH/NOx, and BnOH/H_2O_2 experiments. Tables 6 and 7 shows additional aerosol species with high oxygen
1008 to carbon ratio and/or nitro group. NA: not applicable. [a]: underivatized m/z are given. *: identified with authentic standard.

IUPAC/common nomenclature	Formula	m/z BSTFA (EI)	MW [MW$_{BSTFA}$] (g mol^{-1})	Proposed Structure	Detected
Benzyl alcohol (BnOH)	C_7H_8O	165, 91, 135, 180, 73	108 [180]		GP
Phenol	C_6H_6O	73, 151, 166, 94, 65	94 (166)		GP, PP
Benzaldehyde (BnAld)	C_7H_6O	106, 105, 77, 77, 51	106 (NA)		GP, PP
Benzene-1,2-diol (catechol)	$C_6H_6O_2$	239, 255, 80, 283, 73	110 (254)		PP
Benzoic acid	$C_7H_6O_2$	179, 105, 135, 77, 194	122 (194)		GP, PP
Salicylaldehdye	$C_7H_6O_2$	179, 105, 135, 77, 194	122 (194)		GP
3-Hydroxy benzaldehyde	$C_7H_6O_2$	179, 105, 135, 77, 194	122 (194)		GP
2-Hydroxybenzyl alcohol (salicyl alcohol)	$C_7H_8O_2$	73, 253, 179, 268, 147	124 (268)		GP, PP
4-Hydroxybenzyl alcohol	$C_7H_8O_2$	73, 179, 253, 268, 147	124 (268)		GP, PP
4-Hydroxybenzoic acid (*p*-salicylic acid)	$C_7H_6O_3$	267, 223, 193, 282, 73	138 (282)		PP [H_2O_2]
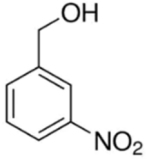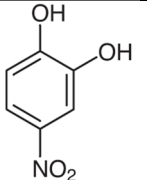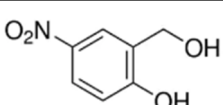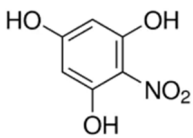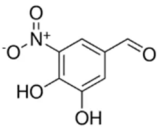
1009

1010 **Table 6.** Highly oxygenated products (O:C > 1.3) identified in benzyl alcohol photooxidation in the presence of NOx, or
1011 H_2O_2. *: identified with authentic standard. *L*-Tartaric acid and *D*-tartaric acid co-elute. The structure of 4-oxo-D-arabonic
1012 acid isomer and 2,3,5-Trihydroxy-4-oxopentanal isomer are shown for trihydroxy-oxo-pentanoic acid, and trihydroxy-
1013 oxo-pentanal, respectively. Four peaks with similar fragments/adducts as pentaric acid were observed.

Nomenclature	Chemical Formulae	O/C Ratio (by wt)	*m/z* BSTFA Derivative (CI-CH4); (EI)	MW (MW$_{BSTFA}$)	Proposed Structure
Epoxysuccinic acid (2 peaks)	$C_4H_4O_5$	1.7	187, 261, 73, 277, 173 73, 173, 261, 129, 143	132 (276)	
2-Hydroxybutanedioic acid* (malic acid)	$C_4H_6O_5$	1.7	233, 335, 73, 307, 351 73, 147, 233, 245, 335	134 (350)	
Trihydroxy-oxo-pentanal (5 peaks)	$C_5H_8O_5$	1.3	73, 275, 203, 349, 393 147, 73, 349, 233, 259	148 (364)	
meso-Tartaric acid*	$C_4H_6O_6$	2.0	423, 321, 277, 439, 73 73, 147, 292, 219, 423	150 (438)	
L-Tartaric acid*	$C_4H_6O_6$	2.0	423, 321, 277, 439, 73 73, 147, 292, 219, 423	150 (438)	
Trihydroxy-oxo-pentanoic acid (8 peaks)	$C_5H_8O_6$	1.6	73, 437, 363, 481, 493 217, 73, 147, 437, 292	164 (452)	
D-Arabinonic acid* (Arabic acid)	$C_5H_{10}O_6$	1.6	361, 217, 73, 435, 525 204, 437, 73, 147, 319	166 (526)	
Pentaric acid* (4 peaks)	$C_5H_8O_7$	1.9	525, 333, 407, 435, 73 73, 292, 189, 407, 525	180 (540)	

1014

1015

1016

1017

1018   **Table 7.** NACs identified in benzyl alcohol photooxidation in the presence of NOx.

Nomenclature	Chemical Formula Rt (min)	*m/z* BSTFA Derivative (CH$_4$-CI) (EI)	MW (MW$_{bstfa}$)	Observed in GP; PP [GP/PP ratio]	Proposed Structure
3-nitrobenzyl alcohol[a]	C$_7$H$_7$NO$_3$ (25.93)	226, 210, 180, 136, 73 210, 180, 165, 194, 73	153 (225)	PP, GP [1.71]	
4-nitrocatechol[a]	C$_6$H$_5$NO$_4$ (30.86)	300, 284, 328, 254, 73 73, 284, 299, 269, 223	155 (299)	PP, GP [0.08]	
2-hydroxy-5-nitro benzyl alcohol[a] (4 isomers)	C$_7$H$_7$NO$_4$ (34.26)	314, 298, 268, 342, 73 298, 283, 191, 314, 73	169 (313)	PP, GP [0.08]	
2-nitro phloroglucinol[a] (4 isomers)[b]	C$_6$H$_5$NO$_5$ (35.62)	388, 372, 416, 428, 73 73, 372, 387, 284, 306	171 (387)	PP	
3,4-dihydroxy-5-nitrobenzyl alcohol (4 isomers)[c]	C$_7$H$_7$NO$_5$ (38.18)	388, 372, 416, 428, 73 73, 224, 3876, 401, 356	185 (401)	PP	

1019   [a]: identified using authentic standards. [b]: Three additional peaks eluted at 33.76, 34.70, 34.76 min with similar mass spectra
1020   as those recorded for 2-nitrophloroglucinol standard were detetcted, and the structure given here is for 2-
1021   nitrophloroglucinol. [c]: Three additional peaks eluted at 35.94, 36.60, 38.18 min with similar mass spectra were detetcted.

1022
1023
1024
1025
1026
1027
1028
1029
1030
1031
1032

1033
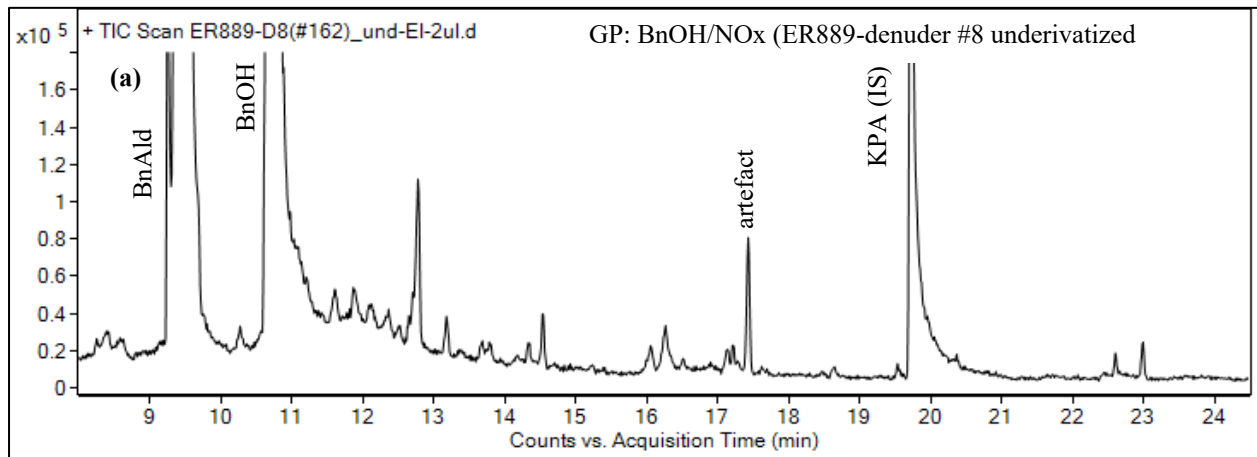
1034
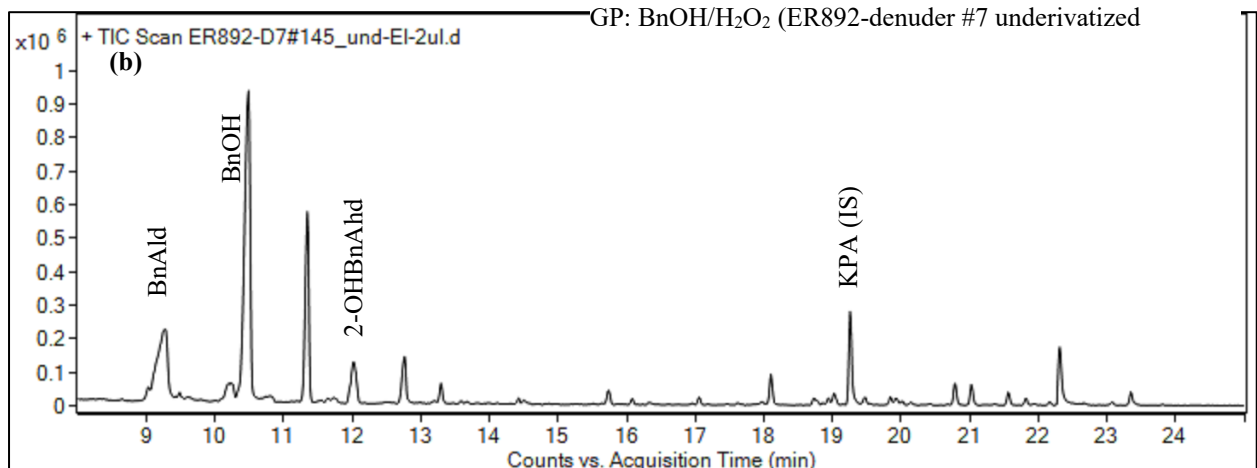
1035
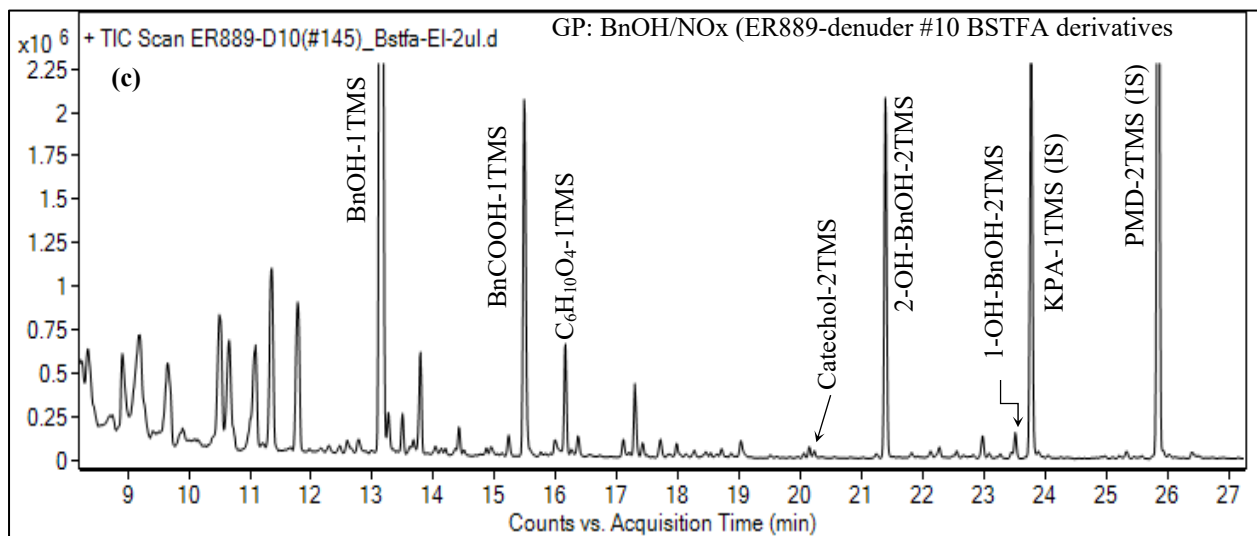
1036 **Figure 1.** Portion of GC-MS total ion chromatogram in EI mode of GP underivatized denuder extract (a) ER-889 (presence of NOx),

1037 (b) ER-892 (absence of NOx), and (c) ER889- (presence of Nox) as BSTFA derivatives.
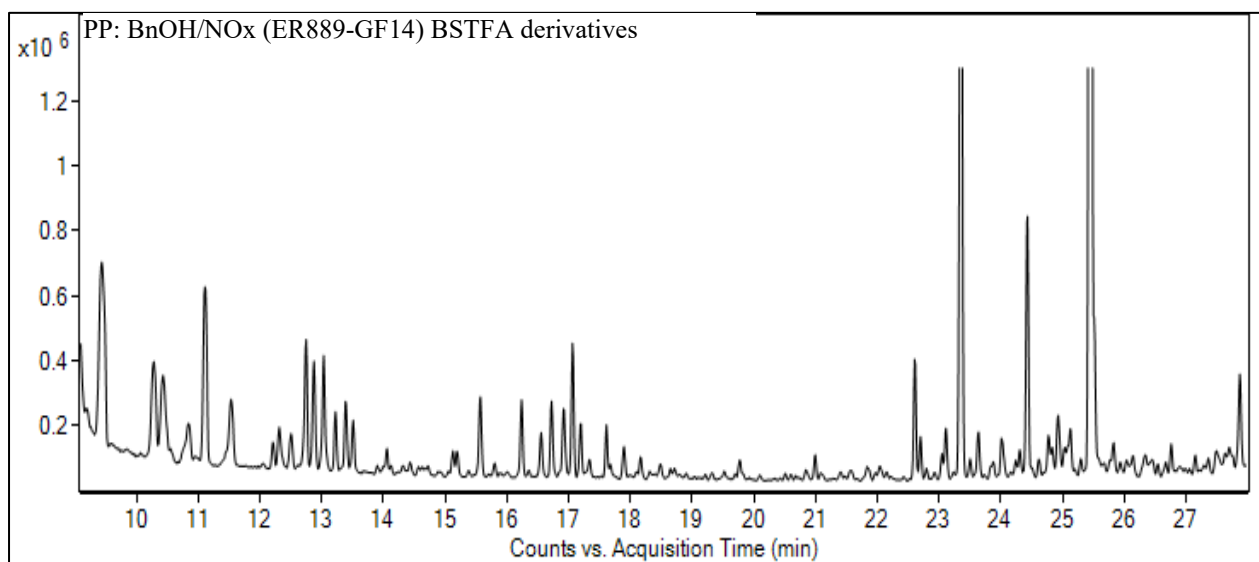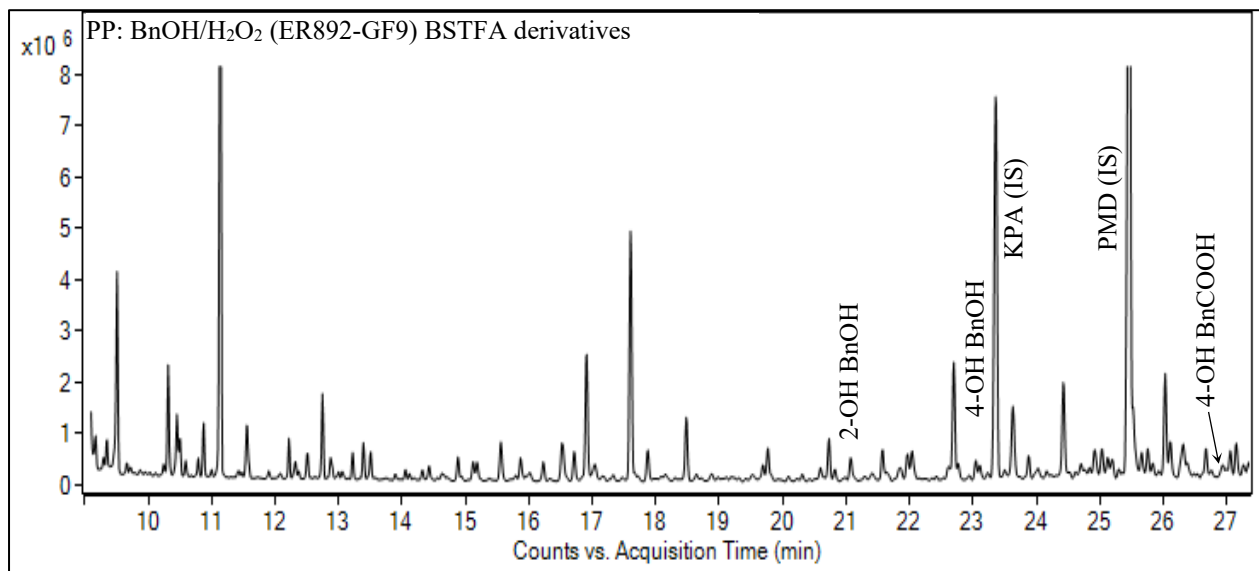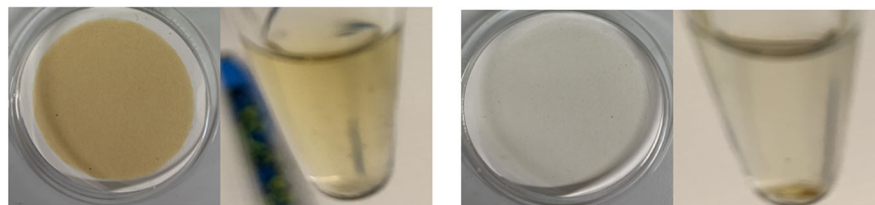
F1: BnOH/NOx   E1: methanol extract   F2: BnOH/H2O2   E2: methanol extract

Figure 2. Portion of GC-MS total ion chromatograms (EI mode) of particle-phase extracts: (top) BSTFA derivatized sample form ER-889 (presence of NOx), (middle) BSTFA derivatives from ER-892 (absence of NOx), (bottom) effect of mixture changes in filter and methanol extract appearance: BnOH/NOx filter (F1); BnOH/H2O2 (F2). The same volume of air was sampled on each filter.
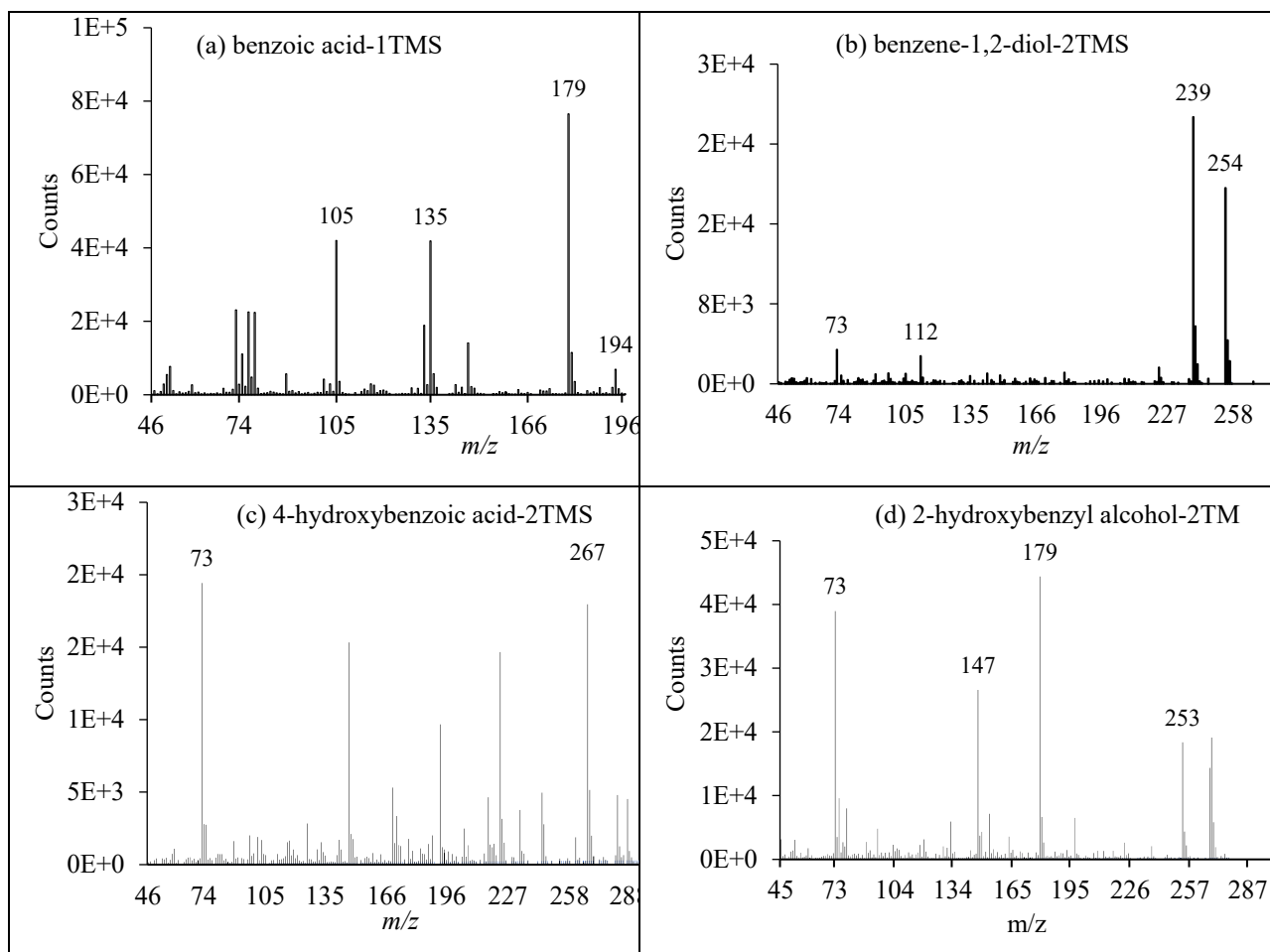
1044   **Figure 3.** Positive EI mass spectra of BSTFA derivatives of selected ring-containing products: benzoic acid, benzene-1,2-diol, 4-
1045   hydroxybenzoic acid; and 2-hydroxybenzyl alcohol.

1046

1047

1048

1049

1050
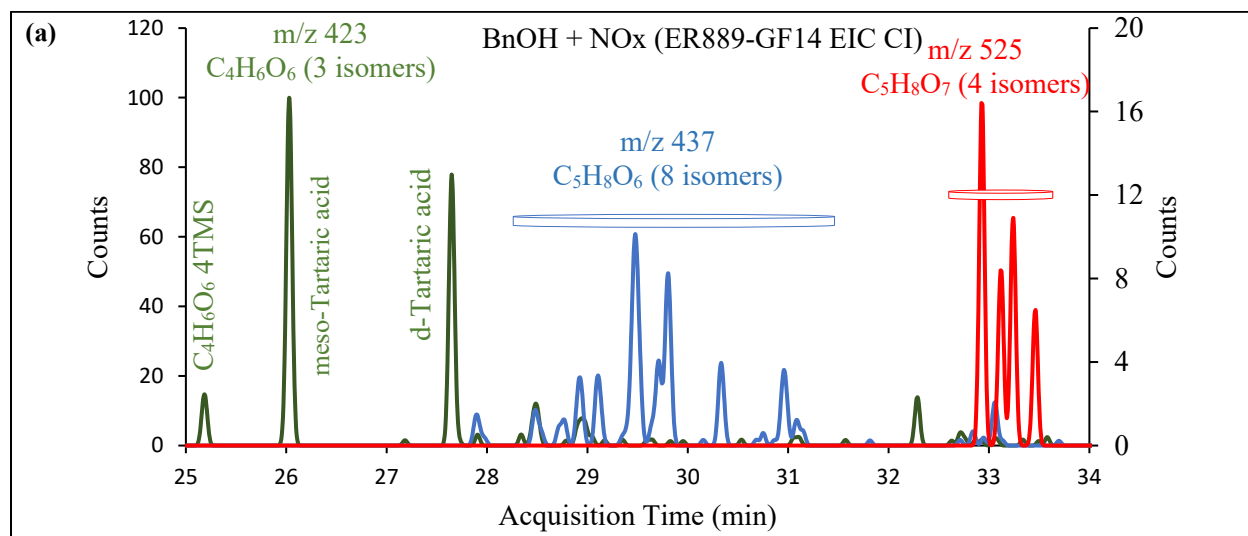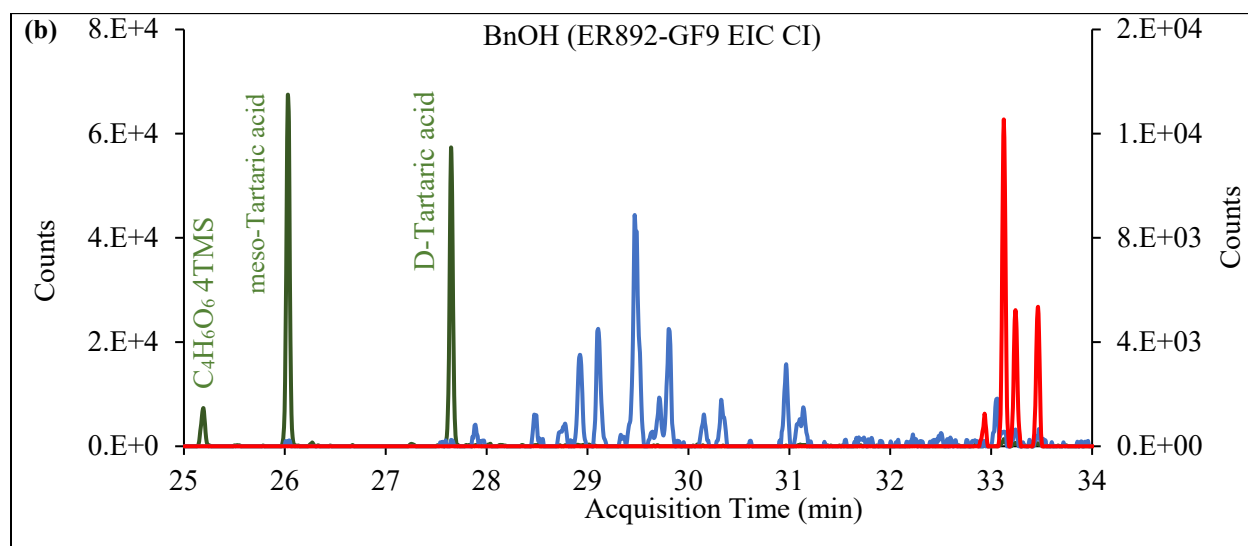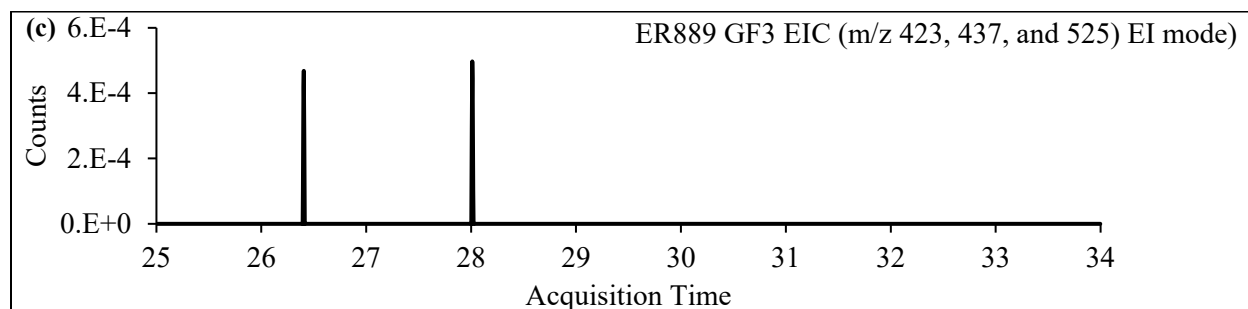
Figure 4. Portion (25-34 min) of GC-MS extracted ion chromatograms (CI-CH₄) at *m/z* 423 (green); m/z 437 (blue); and m/z 525 (red) merged in one chromatogram (a) BnOH in the presence of NOx; (b) BnOH in the presence of H_2O_2 and absence of NOx; (c) Chamber background. Red and top blue: right axis.
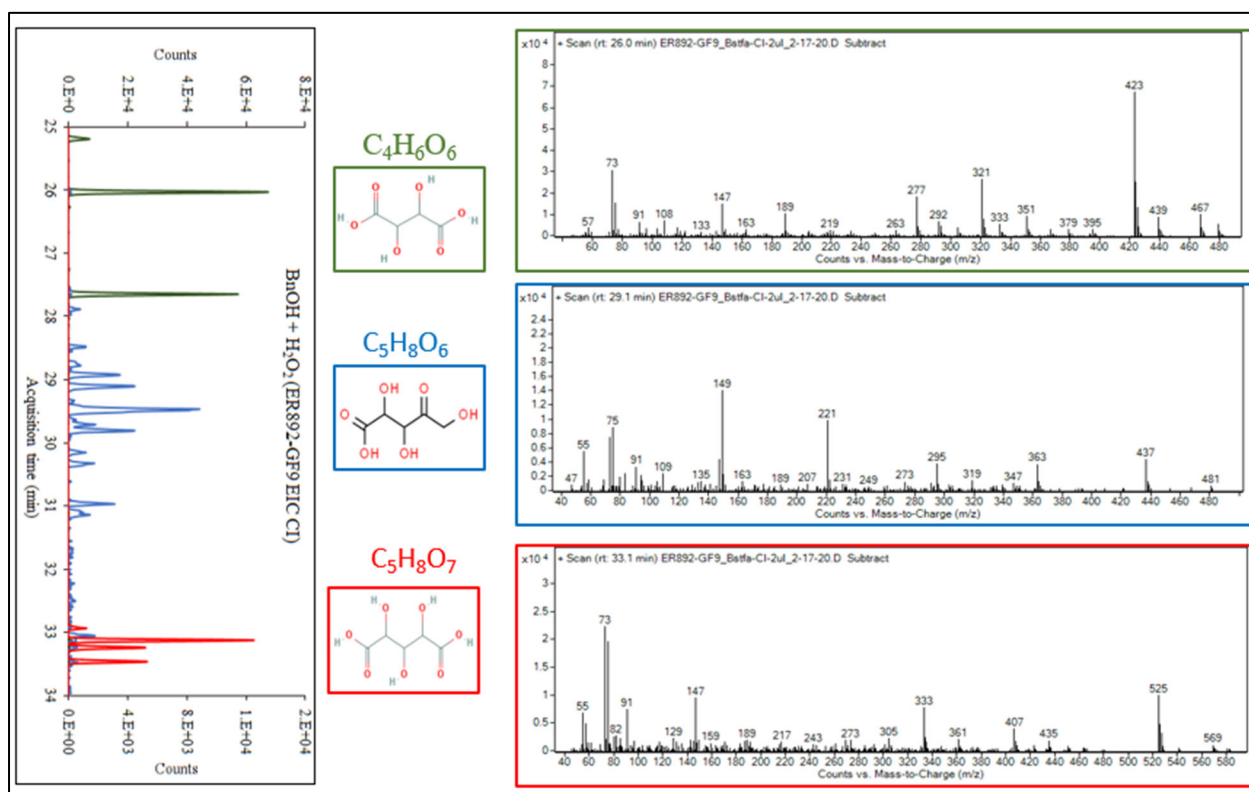
Figure 5. Mass spectra (methane-CI) of ester TMS derivatives of meso-tartaric acid (top right), trihydroxy-oxo-pentanoic acid (middle right), (c) pentaric acid (bottom right), along with the portion of GC-MS extracted ion chromatograms shown in figure 6. Chemical formulae and chemical structure associated with each group is given in the middle column.
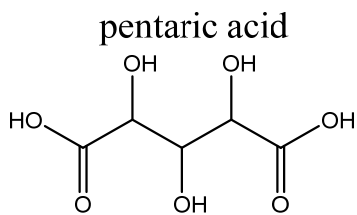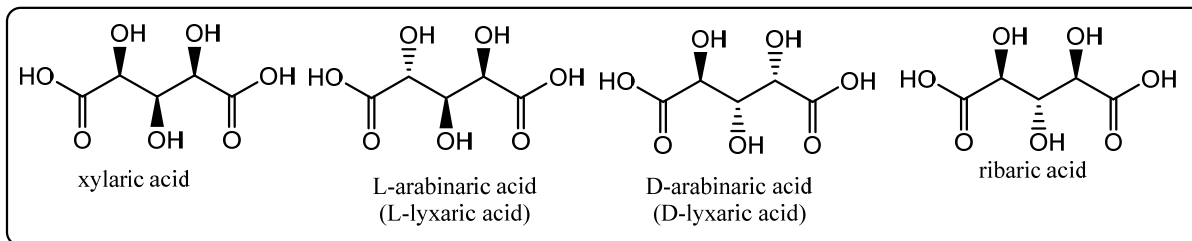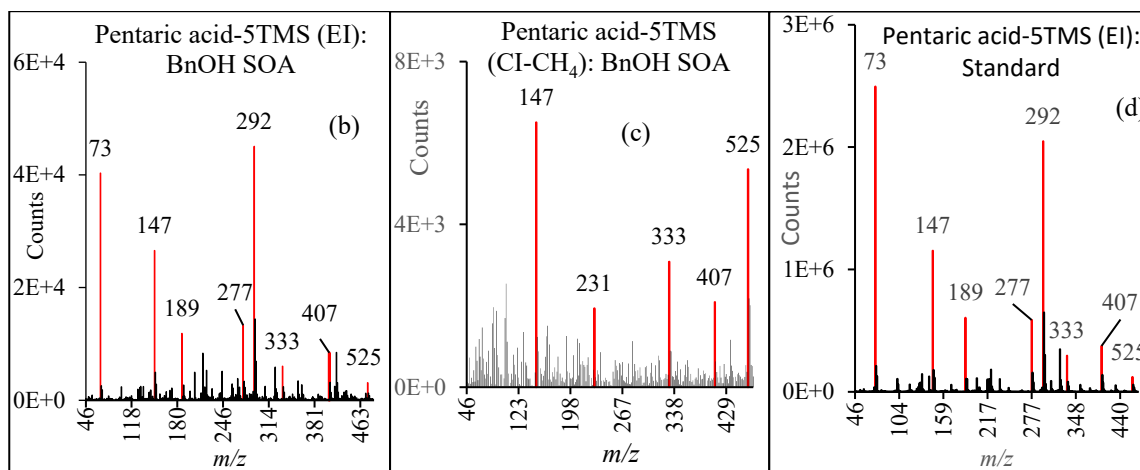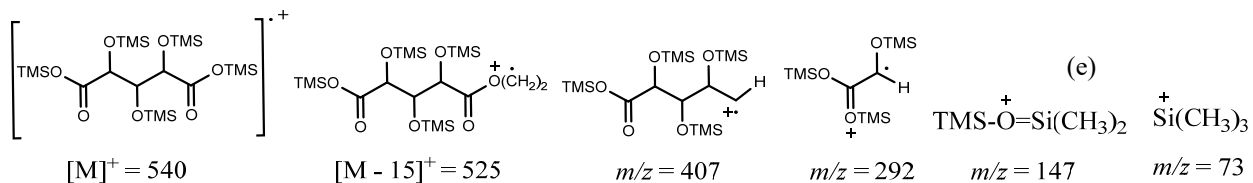
Figure 6. Molecular structures of pentaric acid and its isomers (a); mass spectra of TMS derivatives of pentaric acid acquired for smog chamber SOA (EI: b, CI: c) and authentic standard (d: EI); Major pentaric acid fragments observed in EI mode (e).
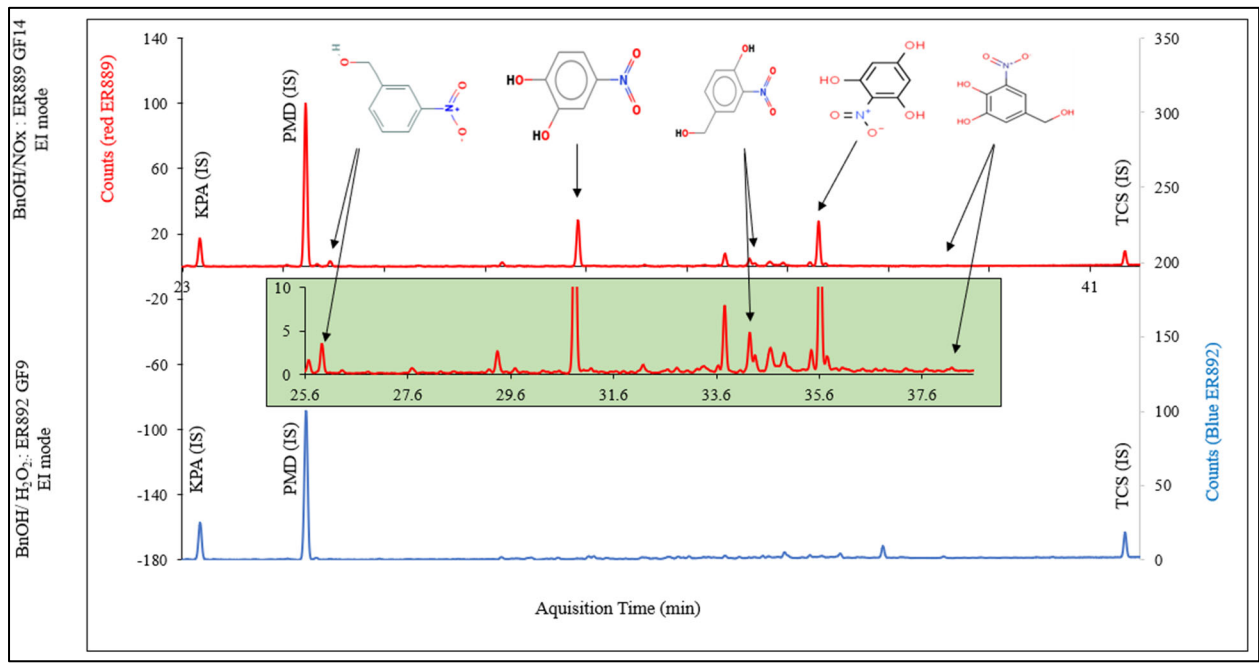
1080

1081 **Figure 7.** Portion of GC-MS extracted ion chromatograms (EI mode) at *m/z* 210, 165 (IS), 299 (IS), 300, 298, 372, 388 associated with

1082 nitroaromatic compounds merged in one chromatogram (red) BnOH in the presence of NOx (ER889); (blue) BnOH in the presence of

1083 H_2O_2 and absence of NOx (ER892).

1084

1085

1086

1087

1088